

Comparing self-consistent GW and vertex corrected G_0W_0 ($G_0W_0\Gamma$) accuracy for molecular ionization potentials

Ming Wen,[†] Vibin Abraham,[†] Gaurav Harsha,[†] Avijit Shee,[‡] K. Birgitta Whaley,[‡] and Dominika Zgid^{*,†,¶}

[†]*Department of Chemistry, University of Michigan, Ann Arbor, Michigan 48109*

[‡]*Department of Chemistry, University of California, Berkeley, California 94720-1460*

[¶]*Department of Physics, University of Michigan, Ann Arbor, Michigan 48109*

E-mail: zgid@umich.edu

Abstract

We test the performance of self-consistent GW and several representative implementations of vertex corrected G_0W_0 ($G_0W_0\Gamma$). These approaches are tested on benchmark data sets covering full valence spectra (first ionization potentials and some inner valence shell excitations). For small molecules, when comparing against state of the art wave function techniques, our results show that full self-consistency in the GW scheme either systematically outperforms vertex corrected G_0W_0 or gives results of at least comparative quality. Moreover, $G_0W_0\Gamma$ results in additional computational cost when compared to G_0W_0 or self-consistent GW . The dependency of $G_0W_0\Gamma$ on the starting mean-field solution is frequently more dominant than the magnitude of vertex correction itself. Consequently, for molecular systems, self-consistent GW performed on imaginary axis (and then followed by modern analytical continuation techniques) offers a more reliable approach to make predictions of ionization potentials.

Introduction

Accurate and computationally accessible simulation of molecules and solids is a major goal when developing new or improving existing computational approaches. Wave function methods such as coupled cluster method (CC)¹⁻⁶ and configuration interaction (CI)⁷⁻⁹ have seen a great success in modeling moderately sized molecules and solids with small unit cells. However, these ab-initio simulations for larger and more complicated systems still remain extremely challenging, mainly due to the high computational scaling.

For larger molecules and periodic systems, methods with lower computational scaling are favorable. Approaches such as density functional theory (DFT)^{10,11} are more efficient in tackling systems with large numbers of electrons. However, these methods often struggle to offer quantitatively accurate predictions when electron correlation plays a significant role. Moreover, for DFT methods there is a lack of a systematic route to improve the results.

Many-body perturbation theory (MBPT) cast into the Green's function language provides an alternative group of ab-initio methods to model electron correlation.¹² Most of these methods such as GW ¹³⁻²³ or Green's function second order (GF2)²⁴⁻²⁸ can be executed with relatively low computational scaling, especially when compared to wave function theories.

Since the diagrammatic Green's function expansions are based on perturbation theory, they also hold a promise of being systematically improvable. In 1965, Hedin proposed a complete set of conjugated equations, detailing the relationships between the Green's function, irreducible polarizability, screened Coulomb interaction, vertex function, and self-energy.¹³ The GW method constitutes a simpler truncated formulation of Hedin's equations of MBPT. A more approximated version of GW theory, namely G_0W_0 , where only the first iteration of the self-consistent loop is performed (vertex function is assumed to be unity), has become one of the most widely applied methodologies in computational electronic structure. While relatively accurate and computationally inexpensive, G_0W_0 still lacks full quantitative accuracy and can qualitatively fail for systems with stronger electron correlations.

One of the proposals of improving G_0W_0 accuracy is the addition of the vertex function

Γ as a correction term to G_0W_0 . Those vertex-corrected methods are commonly referred to as $G_0W_0\Gamma$.^{29–36} Note that in this manuscript, we refer to $G_0W_0\Gamma$ as a general term for the group of methods that involve the vertex correction. When a specific variant of vertex correction is being discussed, we use a specific name for that given variant such as $G_0W_0\Gamma_X$, $G_0W_0\Gamma_0^{(1)}$, or $G_0W_0\Gamma^{(NL)}$, introduced later in the Theory section.

Generally, the vertex correction is expected to address stronger electron correlation (or simply correlation missing at the G_0W_0 level) in both solids and molecules, and improve predictions for the band structure and the photo-electron spectrum. However, the implementations, approximations, and performances of $G_0W_0\Gamma$ vary from one version to another because many different strategies can be used to lower the computational scaling.

The vertex correction will result in addition of new diagrammatic terms to G_0W_0 . Another possible strategy is to avoid adding new diagrams and renormalize the Green’s function lines in the GW expressions. By performing full self-consistency of the Hedin’s equations (excluding the vertex), we can update the Green’s function G and self-energy Σ in each loop, resulting in a fully self-consistent GW description (sc GW).^{37–39}

The formal computational scaling of finite-temperature GW using the Matsubara formalism is $\mathcal{O}(N^6)$, but it can be reduced to $\mathcal{O}(N^4)$ when density fitted integrals are employed.^{39,40} When compared with G_0W_0 , the cost of sc GW differs only by a prefactor depending on the number of iterations required to reach convergence. Multiple variants of the GW self-consistency were introduced in the past. For detailed discussions of these variants, see Refs.^{22,39–44}

Consequently, two proposals can be put forward to improve the accuracy of G_0W_0 results: (i) inclusion of the vertex function directly on top of G_0W_0 (the $G_0W_0\Gamma$ scheme), or alternatively (ii) performing fully self-consistent GW loops (the sc GW scheme). We aim to investigate the performance improvement of these two routes upon G_0W_0 . These comparisons will guide future developments in the Green’s function theories towards robust methods that provide a good compromise between low computational scaling and high accuracy. We

focus our investigations on small molecules because accurate ionization data from ab-initio methods are readily available.

Moreover, we are also interested in this comparison as the reliability of vertex corrections has been a topic of recent discussions in molecular ionization potential (IP) prediction. Berkelbach and Lewis noted that the additional diagrams in the $G_0W_0\Gamma$ scheme did not result in the improvement of the G_0W_0 results, if vertex diagrams were added to the polarizability exclusively, but not to the self-energy.⁴⁵ Multiple works also noticed that vertex-corrected G_0W_0 based on Hartree-Fock references did not improve parent G_0W_0 results.^{33,45,46} However, changing the functional reference to PBE resulted in some improvements reported in in Ref.³³ In the scGW scheme, the Green’s function lines are renormalized in the diagrammatic expansion and the results are not dependent on the initial mean-field.

In this work, we employ our recently introduced finite temperature scGW method^{38,39,43} and compare its results against a few representative $G_0W_0\Gamma$ schemes presented earlier in the literature. We compare against three possible ways of approximating vertex, (i) stochastic methodology developed in the group of Vlček in Ref.,⁴⁷ (ii) $G_0W_0\Gamma_0^{(1)}$ implemented by Wang et al. and presented in Ref.,³³ and (iii) $G_0W_0\Gamma^{(NL)}$ implemented in the Kresse’s group and presented in Ref.³² by Maggio *et al.*

scGW and vertex corrected G_0W_0 methodologies are tested on molecular examples and validated against wave function theories or experimental data. We examine these approaches both for the first and inner valence shell IPs depending on the availability of related data sets. Note that the respective performance of scGW and vertex-corrected GW on electronic gases²¹ and metals⁴⁸ can differ from molecular cases. In this work, we restrict our discussion to the molecular regime unless specified otherwise.

We present our work in this article as follows. In the Theory section, we provide a concise introduction to finite temperature scGW and a brief review of recent developments in adding the vertex correction to G_0W_0 . The Computational Procedure section describes the general calculation protocol we used to conduct predictions. The Results section contains findings

of this work. We summarize our findings and outlooks in the Conclusions section.

Theory

Hedin's equations

A set of self-consistent equations detailing the relationship among the self-energy, Green's function, screened Coulomb interaction, and irreducible polarizability in many-electron systems was formulated in Hedin's foundational article.¹³

In the derivation of Hedin's equations, a bare Coulomb interaction v is affected (or "screened") by the many-electron environment. The screened Coulomb interaction W is defined as

$$W(12) = v(12) + W(13)P(34)v(42), \quad (1)$$

where numeric compact indices are employed as a shorthand to represent the state of space-time and spin as $1 = (\mathbf{x}_1, \sigma_1, t_1)$. Integration over repeated indices is assumed. The irreducible polarizability is defined as

$$P(34) = iG(45)G(64)\frac{\delta G^{-1}(56)}{\delta V(3)}, \quad (2)$$

where V is the time evolution operator. The functional derivative $\delta G^{-1}(56)/\delta V(3)$ is called the vertex function, and expressed as

$$\begin{aligned} \Gamma(12; 3) &\equiv -\frac{\delta G^{-1}(12)}{\delta V(3)} = \delta(12)\delta(13) + \frac{\delta \Sigma(12)}{\delta V(3)} \\ &= \delta(13)\delta(23) + \frac{\delta \Sigma(12)}{\delta G(45)}G(46)G(75)\Gamma(67; 3). \end{aligned} \quad (3)$$

The inclusion of vertex function can be viewed as the information about the interaction among electrons and holes.^{49,50}

In the original formulation, evaluating the exact vertex function significantly increases

the computational cost because it is difficult to calculate a four-index functional derivative. If the vertex function is truncated at the zeroth order in Eq. (3) as $\Gamma(12; 3) \approx \delta(12)\delta(13)$, then the self-energy Σ and the reduced polarizability P can be calculated without evaluating the functional derivative as

$$\begin{aligned}\Sigma(12) &= iW(13)G(14)\Gamma(42; 3) \\ &\approx iG(12)W(12),\end{aligned}\tag{4}$$

$$\begin{aligned}P(12) &= -iG(23)G(42)\Gamma(34; 1) \\ &\approx -iG(12)G(21).\end{aligned}\tag{5}$$

The name GW approximation (GWA) was coined to signify the exclusion of vertex function in Hedin's equations.^{13,16} The GWA scheme is depicted by the trapezoidal loop in the right diagram of Figure 1.

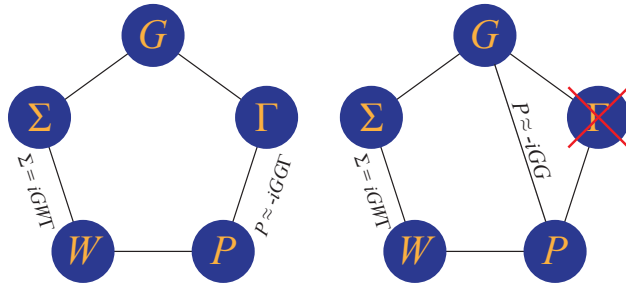


Figure 1: Left: The self-energy, Green's function, vertex function, irreducible polarizability, and screened Coulomb interaction conjugated by Hedin's equations. Right: The GW approximation loop of Hedin's equations without inclusion of the vertex function.

G_0W_0 and self-consistent GW

GWA can be executed in two ways. One of them called G_0W_0 is the first iteration of the Hedin's equations loop without the inclusion of the vertex function where the zeroth order Green's function G_0 is evaluated using a mean-field Hamiltonian (Hartree-Fock or DFT).

Then the Green's function is used to evaluate the self-energy. Usually, only the diagonal elements of the self-energy matrix are evaluated and the quasiparticle (QP) approximation is then employed to afford spectral quantities.²³

Fully self-consistent *GW* (*scGW*) is executed if all the quantities (excluding the vertex function) described by Hedin's equations are iterated until self-consistency. For the implementation details of *scGW* as performed in the Zgid group, we encourage the reader to consult Ref.⁵¹ for molecular problems, Refs.^{38,39,52} for periodic solid problems, and Ref.⁴³ for relativistic problems in periodic solids.

In our finite temperature *scGW* implementation, we express the frequency/time dependent quantities on an imaginary axis grid.⁵³⁻⁵⁶ No diagonal approximation to the self-energy is used and all the matrix elements of self-energy for all the frequencies are evaluated and included in the self-consistent equations. The total self-energy in *scGW* is expressed as

$$\Sigma^{GW}[\mathcal{G}](i\omega) = \Sigma_{\infty}^{GW}[\mathcal{G}] + \tilde{\Sigma}^{GW}[\mathcal{G}](i\omega), \quad (6)$$

where $\Sigma_{\infty}^{GW}[\mathcal{G}]$ is the static part of self-energy evaluated using the first order diagrams (Hartree and exchange) employing the correlated one-body density matrix, and $\tilde{\Sigma}^{GW}[\mathcal{G}](i\omega)$ is the frequency-dependent dynamical part of self-energy. Both self-energy parts, dynamic and static, depend on Green's function and are evaluated iteratively until achieving self-consistency.

In our implementation, the density-fitting approximation⁵⁷ is used to decompose two-electron integrals. Overall, the computational cost of our *scGW* scales as $\mathcal{O}(N_{\tau}N_{\text{orb}}^2N_{\text{aux}}^2)$, where N_{τ} is the number of imaginary time grid points, N_{orb} is the number of orbitals in the problem, and N_{aux} is the number of auxiliary basis functions used in the density fitting procedure.

No QP approximation is evoked to evaluate spectral quantities in our version of *scGW*. To yield spectral information, the finite-temperature Green's function from the imaginary

axis is continued to the real frequency axis with the help of the Nevanlinna analytical continuation technique introduced by Fei *et al.*^{58,59} The spectral function can be derived from the continued Green’s function as

$$\mathcal{G}(i\omega) \xrightarrow[\text{analytical continuation}]{\text{Nevanlinna}} A(\omega) = -\frac{1}{\pi} \text{Im} [\text{Tr}[G(\omega)]] . \quad (7)$$

Spectral functions rendered by Nevanlinna analytical continuation are positive and normalized by definition, which helps to resolve the isolated ionization peaks in the PES. We use the notation “scGW” to refer to our finite-temperature implementation which exactly follows the procedure of self-consistent Hedin equation without including the vertex. This procedure is then followed by the Nevanlinna analytical continuation. Our scGW scheme should contrasted to other self-consistency schemes such as the ones proposed by Schilfgaard-Kotani-Faleev,^{60,61} and eigenvalue-self-consistent GW.⁶² These schemes constitute a further departure from Hedin’s original scheme.

Practical implementations of vertex correction

It is believed that introducing the vertex function Γ as a correction term on top of GWA can improve its accuracy. The rigorous evaluation of vertex function is difficult due to the presence of the four-point functional derivative ($\delta\Sigma/\delta G$) in Eq. 3 and due to the necessity of iterative self-consistent evaluation of both self-energy Σ and irreducible polarizability P since they involve Γ in their respective Eqs. 4 and 5. Consequently, in practical implementations of the vertex correction, many approximations are introduced to lower the computational cost and make such evaluations viable.

It is frequently argued that scGW overestimates band gaps.^{21,63} Thus G_0W_0 , which benefits from the error cancellation between the mean-field starting point and a subsequent GW evaluation, is used as an affordable alternative. In this approximation, Γ is evaluated on top of G_0W_0 resulting in a $G_0W_0\Gamma$ method. However, even in this simplified scenario further

approximations are necessary to make the final evaluation of $G_0W_0\Gamma$ possible. Here, we summarize recent developments of practical $G_0W_0\Gamma$ implementations.

Reining and coworkers introduced the ρ/G -approach,^{30,64,65} in which a two-part vertex correction was proposed as

$$\begin{aligned}\Gamma(12; 3) &= \delta(13)\delta(23) + \delta(12)f_{xc}^{\text{eff}}(14)P(43) \\ &+ \Delta\Gamma(12; 3),\end{aligned}\tag{8}$$

$$\Delta\Gamma(12; 3) = \left[\frac{\delta\Sigma_{xc}(12)}{\delta\rho(4)} - \delta(12)f_{xc}^{\text{eff}}(14) \right] P(43).\tag{9}$$

The first two terms in Eq. 8 are defined as a “local” part while $\Delta\Gamma$ is called the “non-local” term because $\Delta\Gamma$ has zero contribution to P .

In both the local and non-local parts, f_{xc}^{eff} is included. It serves as an auxiliary effective function used to obtain P easily from only two-point quantities. f_{xc}^{eff} has an exact definition which involves a three-point kernel $\delta\Sigma_{xc}/\delta\rho$, but is often approximated with v_{xc} ($\delta\Sigma_{xc}/\delta\rho \approx \delta v_{xc}/\delta\rho$) retrieved from the starting mean-field calculation. Such a local vertex correction is relatively inexpensive to compute, but alone it is insufficient in improving G_0W_0 accuracy.^{64,66,67}

Kresse and co-workers^{32,68} reported their version of non-local vertex correction implementation with the re-formulated four-point notation, given by

$$\begin{aligned}\Gamma(1234) &= \delta(13)\delta(24) \\ &+ i \frac{\delta\Sigma_{xc}(12)}{\delta G(56)} G(57)G(86)\Gamma(7834),\end{aligned}\tag{10}$$

instead of the Hedin’s original three-point one. The four-point kernel is approximated as

$$i \frac{\delta\Sigma_{xc}(12)}{\delta G(56)} \approx -\delta(26)\delta(15)\delta(t_1, t_2)W^{\text{RPA}}(\mathbf{x}_1, \mathbf{x}_2, \omega = 0),\tag{11}$$

where W^{RPA} is the screened Coulomb interaction, estimated with the random phase approximation employing the frequency-dependent exact-exchange kernel f_x (RPAX).^{69,70} Moreover, the static estimation of $\omega = 0$ is applied,^{13,71} assuming that the kernel is relatively frequency independent. Even with RPAX, it is still preferred to evaluate the approximated kernel with a HF starting point instead of a GW reference state. By doing so, screened Coulomb interaction W^{RPA} could be further simplified as the bare Coulomb interaction $v(\mathbf{x}_1, \mathbf{x}_2)$ as

$$i \frac{\delta \Sigma_{\text{xc}}(12)}{\delta G(56)} \approx -\delta(26)\delta(15)\delta(t_1, t_2)v(\mathbf{x}_1, \mathbf{x}_2). \quad (12)$$

The implementation of $G_0W_0\Gamma$ scales formally as $\mathcal{O}(N^6)$.³² In this work we refer to this implementation as $G_0W_0\Gamma^{\text{(NL)}}$, where “NL” stands for “non-local”.

Wang *et al.*³³ reported vertex function truncated at the first order. By plugging in GW approximated self-energy Σ^{GW} in the $\delta\Sigma/\delta G$ kernel as

$$\begin{aligned} \frac{\delta \Sigma(12)}{\delta G(45)} &\approx \frac{\delta \Sigma^{\text{GW}}(12)}{\delta G(45)} = \frac{\delta [iG(12)W(12)]}{\delta G(45)} \\ &= i\delta(14)\delta(25)W(12) + G(12)\frac{\delta W(12)}{\delta G(45)}. \end{aligned} \quad (13)$$

Inserting the approximated expression into Eq. (3), it becomes

$$\begin{aligned} \Gamma(12; 3) &= \delta(13)\delta(23) \\ &\quad + iW(12)G(16)G(72) \underbrace{\Gamma(67; 3)}_{\approx \delta(63)\delta(73)} + \dots \end{aligned} \quad (14)$$

By truncating any terms involving order equal to or higher than $\mathcal{O}(W^2)$, the first order vertex function is equivalent to the full second-order self-energy in terms of W (FSOS- W) as

$$\begin{aligned} \Gamma^{(1)}(12; 3) &\approx \delta(13)\delta(23) \\ &\quad + iW(12)G(13)G(32). \end{aligned} \quad (15)$$

Since only a single iteration is performed to evaluate such a vertex, a subscript of 0 is added to $\Gamma^{(1)}$. The computation cost for $G_0W_0\Gamma_0^{(1)}$ formally scales as $\mathcal{O}(N^5)$.³³

Vlček⁷² utilized the non-local exchange term in the starting mean-field calculation for the G_0W_0 method to construct an approximated non-local vertex function Γ_X . In this work, the four-point derivative kernel is approximated as

$$\begin{aligned} \frac{\delta\Sigma_{\text{total}}(12)}{\delta G(45)} &\approx \frac{\delta[\Sigma_{\text{hartree}}(12) + \Sigma_{\text{exchange}}(12)]}{\delta G(45)} \\ &= -\nu(25)\delta(45)\delta(12) + \nu(12)\delta(52)\delta(41), \end{aligned} \tag{16}$$

where $\nu(12) = \frac{\delta(t_1-t_2)}{|r_1-r_2|}$. In the evaluation process of Γ_X , a stochastic sampling method, instead of the commonly used deterministic one, is used to further minimize computational cost, which gives the evaluation of Γ_X a sub-linear computational scaling.⁷² We refer to this approach simply as $G_0W_0\Gamma_X$ for clarity, but readers should note its stochastic nature.

To summarize, the approximations often used to implement vertex corrections can be categorized by five major categories: (i) estimation of $\delta\Sigma/\delta G$ kernel; (ii) truncation of Γ , or approximation of Γ with diagrammatic approaches; (iii) correction of Σ only (no correction of P); (iv) operation only on the diagonal elements of certain matrices; (v) avoidance of full self-consistency. Even though all these variants are under the same name of ‘‘vertex corrections’’, their practical implementations can be significantly different from one to another.

In this article, we compare the performance of our scGW with $G_0W_0\Gamma_X$, $G_0W_0\Gamma_0^{(1)}$, and $G_0W_0\Gamma^{(\text{NL})}$.

Computational Procedure

Geometries for molecules within the $GW100$ set⁷³ were obtained from Ref.⁷⁴ Any additional molecules not included the $GW100$ set were selected from the G2 data set.⁷⁵ The additional G2 geometries were taken from Ref.⁷⁶

All scGW calculations were performed on the imaginary time and frequency axes using

our implementation reported in Ref.³⁹ For the starting mean-field calculations, we use both HF and DFT (PBE functional).⁷⁷ We employed the inverse temperature of $\beta = 1000 E_h^{-1}$, which corresponds to temperature $T = 315.8$ K. To render the spectral function from our results on the imaginary frequency axis, converged Green’s functions from scGW are continued to the real frequency axis with Nevanlinna analytical continuation technique.^{58,59} This procedure allows us to identify the first and inner valence shell IP values from the spectral function peaks.

In some cases, we provide the complete basis set (CBS) limit^{78,79} using our scGW results. In such cases, we extrapolate the results with respect to the inverse of the numbers of orbitals that vary with the basis set size. The function is $f(n) = E_\infty^{\text{IP}} + kn^{-1}$, in which E_∞^{IP} is the extrapolated IP value and n is the number of basis functions.⁸⁰

For the G_0W_0 calculations that are reported from our code, we follow the same imaginary axis methodology. We transform the first iteration of scGW self-energy (on the Matsubara axis) to the molecular orbital basis corresponding to the initial mean-field solution (HF or PBE). We then use the Padé analytic continuation,⁸¹ implemented in the PySCF quantum chemistry package,^{82,83} to obtain the self-energy on the real frequency axis. Ionization potential and other quasiparticle excitations are then calculated by solving the quasiparticle equation,

$$\epsilon_p = \epsilon_p^0 + \langle \phi_p | (\Sigma(\epsilon) - v_{xc}) | \phi_p \rangle, \quad (17)$$

where $\langle \phi_p | \Sigma(\omega) | \phi_p \rangle$ is the analytically continued diagonal part of the self-energy, and v_{xc} is the Hartree plus exchange-correlation potential of the corresponding mean-field reference. $G_0W_0\Gamma$ results and statistical criteria in the Results section are either cited or calculated from data reported in relevant literature.

Other input parameters for our calculations (basis set, starting mean-field, *etc.*) vary to facilitate different comparisons. See corresponding subsections in the Results section and Supporting Information for a more detailed description.

Results

We employ the finite-temperature *scGW* method to determine molecular IPs and conduct a comparative analysis of its performance against previously established vertex-corrected *GW* results. To ensure that G_0W_0 and *scGW* from our code can be directly compared with the *GW100* benchmark data, we first inspect the validity of our finite-temperature *GW* by comparing it with past *GW* implementations in Fig. S4 of the Supporting Information. This test demonstrates that the density fitting procedure used in our *GW* implementation, and necessary analytical continuation techniques to obtain spectral data, have no significant bearing on accuracy of our data when compared against the *GW100* benchmark data.

In this section, we first compare our *scGW* results and the valence shell excitations obtained for a stochastic implementation of $G_0W_0\Gamma_X$.⁴⁷ We then move on to focus on only the first IP peaks for which more data are available. To this end, we compare the first-order vertex corrected $G_0W_0\Gamma_0^{(1)}$ method with our *scGW* results for the *GW100* dataset.³³ Similarly, we compare *scGW* to $G_0W_0\Gamma^{(NL)}$ for another set of 29 molecules.³² These results are compared with either highly accurate theoretical reference or experimental benchmark data.

Comparison of *scGW* and stochastic $G_0W_0\Gamma_X$ for valence shell excitations

The objective of this subsection is to compare the IP peaks obtained from our *scGW* implementation to stochastic $G_0W_0\Gamma_X$ as implemented and presented by Vlček and co-workers.⁴⁷ To do so, for five small systems, we look at the IP peaks arising from both the first (or the highest occupied molecular orbital, i.e. HOMO) and the inner valence shell excitations: H_2O , N_2 , NH_3 , C_2H_2 , CH_4 and three additional systems: CO , HF and C_2H_4 .

To establish an equal footing for comparing the two methods, we use the same basis sets, extrapolation technique and molecular geometries as in Ref.⁴⁷ That is, we perform calcula-

tions in aug-cc-pVXZ ($X = D, T, Q$) basis sets^{84–86} and use HF data as initial inputs for the GW calculations. Final sc GW results are extrapolated to the basis set limit in a given basis set family.⁸⁰ We report the first few IP peaks for each molecule so that non-degenerate isolated energy levels can be clearly differentiated. Results from both sc GW and stochastic $G_0W_0\Gamma_X$ are compared against reference data from adaptive sampling configuration interaction (ASCI)^{87,88} method, also reported in Ref.⁴⁷

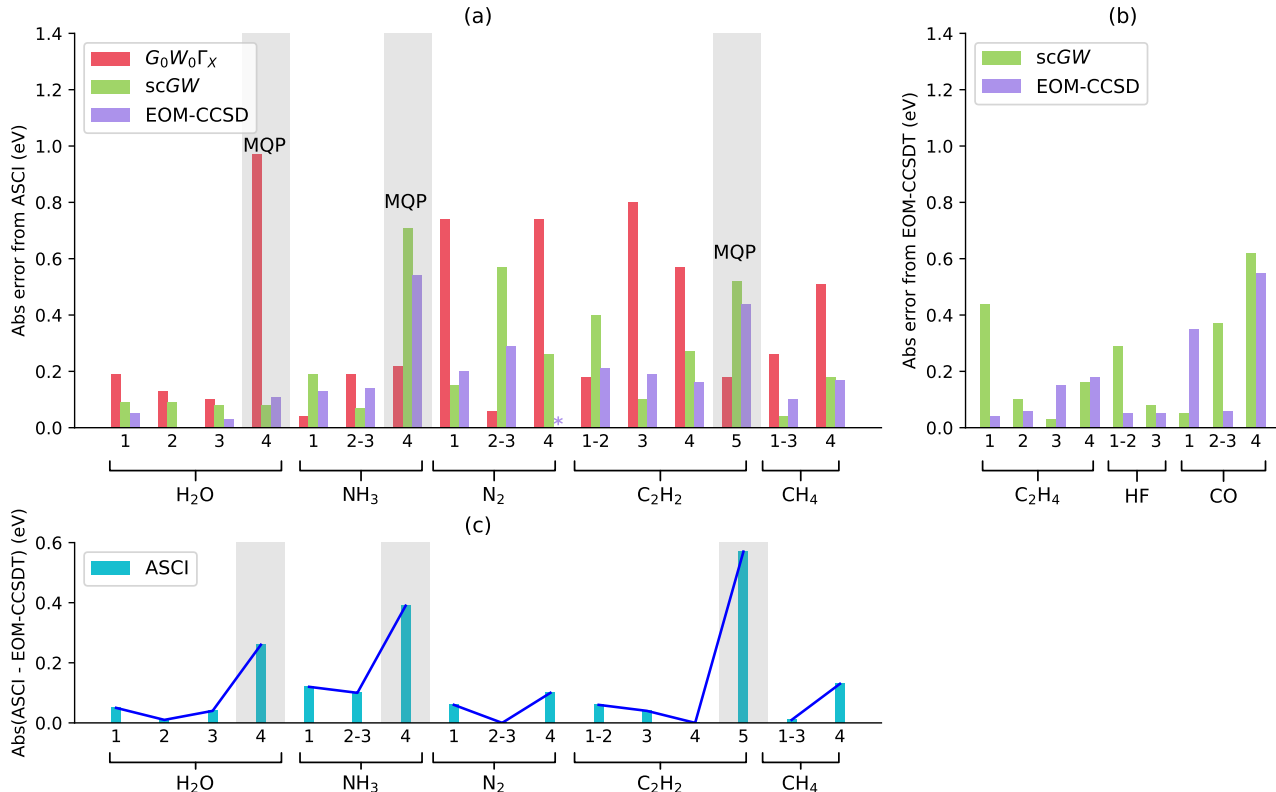


Figure 2: (a) Absolute errors of $scGW$, $G_0W_0\Gamma_X$,⁴⁷ and EOM-CCSD predictions of the first and inner shell ionization peaks as compared with ASCII benchmarks. Note that the bar signified with a purple “*” sign means that EOM-CCSD calculation did not converge and the absolute error is not necessarily zero. Shaded areas are within the multi-quasiparticle peak (MQP) regime. (b) Additional molecules calculated with $scGW$ and EOM-CCSD compared with EOM-CCSDT benchmarks. (c) Absolute errors between ASCII and EOM-CCSDT benchmarks.

In Fig. 2(a), we plot IP peaks computed by stochastic $G_0W_0\Gamma_X$, $scGW$ and EOM-CCSD compared against ASCII benchmarks for the 16 excitations from the 5 systems. Out of the total 16 values reported, $scGW$ yields more accurate data than $G_0W_0\Gamma_X$ for 11 peaks.

However, out of the five peaks where $G_0W_0\Gamma_X$ is better than $scGW$, only for the following three peaks, the difference is more than 0.2 eV: the fourth ionization peak of ammonia, the second/third peaks of N_2 , and the fifth peak of acetylene. For the IP data in Fig. 2(a), the mean absolute error (MAE) with respect to ASCI for $scGW$ is 0.24 eV, and for stochastic $G_0W_0\Gamma_X$ is 0.37 eV. Compared with a 1.47 eV MAE given by G_0W_0 , both $scGW$ and $G_0W_0\Gamma_X$ yield inner excitations with much better accuracy.

In addition to the ASCI method, we also compare our results to equation of motion coupled cluster (EOM-CC)^{89–93} hierarchy. EOM-CC methods are systematically improvable when adding more excitations and hence here we use EOM-CCSD and EOM-CCSDT values. All EOM-CC calculations were performed using CFOUR quantum chemistry package.⁹⁴ Both EOM-CCSD and EOM-CCSDT were performed with aug-cc-pVQZ basis and not extrapolated to the basis set limit. In Fig. 2(c), we look at the difference between inner IPs predicted by EOM-CCSDT and ASCI benchmarks. We observe that the two methods are generally in good agreement with each other (see Table. SI in the Supporting Information). Therefore, EOM-CCSDT could also be used as a benchmark against which GW results can be compared. Discrepancies between ASCI and EOM-CCSDT tend to increase for deep inner excitations, it remains unclear which of the two methods is more accurate.

Moreover, the comparison allows us to assess the $scGW$ method against different levels of excitations used in EOM-CC, i.e. EOM-CCSD and EOM-CCSDT. This is helpful for understanding the accuracy that can be expected from $scGW$ for IP predictions.

In Fig. 2(b), we compare the ionization peaks from $scGW$ and EOM-CCSD for ethylene (C_2H_4), hydrogen fluoride (HF) and carbon monoxide (CO). For these systems, we employ EOM-CCSDT results in the aug-cc-pVQZ basis-set as reference. Overall, based on the results in panels (a) and (b) of Fig. 2, as well as additional data in Fig. S3 of Supporting Information, we deduce that $scGW$ is similar in accuracy as EOM-CCSD. This similarity is not surprising as connections between GW , RPA, and coupled cluster theory have been well studied.^{95–99} However, it is worth noticing that EOM-CCSD data were difficult to obtain

due to convergence problems for some of the inner peaks while *scGW* converged without any difficulty. It is also worth mentioning that for the 4th peaks of H₂O and N₂, $G_0W_0\Gamma_X$ gave relatively poor results. For H₂O and N₂, *scGW* gave very good results, confirming that the difficulty in illustrating these IPs comes from lack of optimization of orbitals in $G_0W_0\Gamma_X$ and not necessarily from the presence of strong correlation. Only the 4th peak of nitrogen displays signs of strong correlation which is not recovered by $G_0W_0\Gamma_X$, and also in EOM-CCSD due to lack of complete convergence.

Further analyzing the results in Fig. 2, the IP data, particularly in panel (a), can be separated into two regimes: (i) single, individual quasiparticle (SQP) and (ii) multi-quasiparticle (MQP).^{47,100} For SQPs, the quasiparticle (or the ionization) peak carries most of the spectral weight. Such peaks can be recovered accurately by *GW* methods.¹⁰¹ On the other hand, for MQP, a significant amount of spectral weight is transferred to satellite features, often referred to as shake-up satellites in molecules.⁴⁷ Mean-field and perturbative methods such as DFT and *GW* are not adept in describing MQPs, as one needs to account for complicated interactions among many excited states.⁵⁰ The general belief is that one can obtain better results for the MQPs by adding higher-order quantum corrections via inclusion of the vertex term, which describes dynamical two-particle correlations.⁴¹ However, when looking at the accuracy of the fully self-consistent *GW* in Fig. 2, we observe that both peaks in the SQP and MQP regimes are well recovered by *scGW*. Therefore, at least based on the examples considered here, we can confidently say that achieving full self-consistency in *GW* provides results that are equally, if not more, accurate than $G_0W_0\Gamma$. While both methods provide significant improvements over G_0W_0 , one could argue that *scGW* is more advantageous over $G_0W_0\Gamma$ as it provides access to other thermodynamic quantities such as total energy, entropy, *etc.*, in addition to the reliable IP prediction and it is independent of the starting point.

Consequently, at least for the examples listed in Fig. 2(a), the vertex correction seem to be unnecessary and very good results can be obtained by employing *scGW* alone. To confirm the points observed above, we plotted spectral functions for selected molecules in

the Supporting Information (see Fig. S1 and S2). We observe that scGW also produces similar complicated MQP regime peak structures as reported in Ref.⁴⁷

Comparison of scGW and $G_0W_0\Gamma_0^{(1)}$ for first IP peaks

Here, we compare the performance of our scGW to $G_0W_0\Gamma_0^{(1)}$ as implemented by Wang et al. and presented in Ref.³³ for the GW100 dataset.^{20,73,102,103} This comparison is done only for the first ionization potential peaks, where molecular data sets are more readily available. To ensure that our scGW data can be compared against the $G_0W_0\Gamma_0^{(1)}$ data, we evaluated our scGW in the same basis set, *i.e.*, def2-TZVPP. For similar reason, for G_0W_0 data, we compare both Hartree-Fock and PBE as mean-field starting points for GW calculations.

In Fig. 3, we list the first IPs for the GW100 molecular data set. In the top panel, we compare the scGW and $G_0W_0\Gamma_0^{(1)}$ errors in IPs based on both the PBE and HF starting points. In the bottom panel, we compare IPs for scGW and G_0W_0 method based on two starting points used in the top panel. All the results are plotted as errors with respect to $\Delta\text{CCSD(T)}$ reference values.¹⁰⁴

By categorizing the GW100 molecules into ten groups, we observe that scGW produces low and consistent errors for hydrides, halogenides, and most oxides. For dimers, hydrocarbons, and aromatics, the errors is higher. For compounds involving bonds with strong polar or ionic character (e.g., CF_4 , SO_2 , and MgO) scGW displays larger errors. Unsaturated bonding character (P_2 , As_2 , BN , HCN) also contributes to abnormal errors.

In the bottom panel of Fig. 3, we observe that scGW improves one-shot G_0W_0 calculations. While the MAE of $G_0W_0\text{@HF}$ is similar to the one of scGW, we see that the majority of errors for scGW comes from nucleobases and MgO . In contrast, $G_0W_0\text{@PBE}$ displays many outliers for multiple system groups.

In the top panel of Fig. 3 and Fig. 4, we observe that adding vertex corrections to $G_0W_0\text{@HF}$ (denoted as $G_0W_0\Gamma_0^{(1)}\text{@HF}$) makes the results consistently worse, while adding vertex correction to $G_0W_0\text{@PBE}$ (denoted as $G_0W_0\Gamma_0^{(1)}\text{@PBE}$) improves the results, making

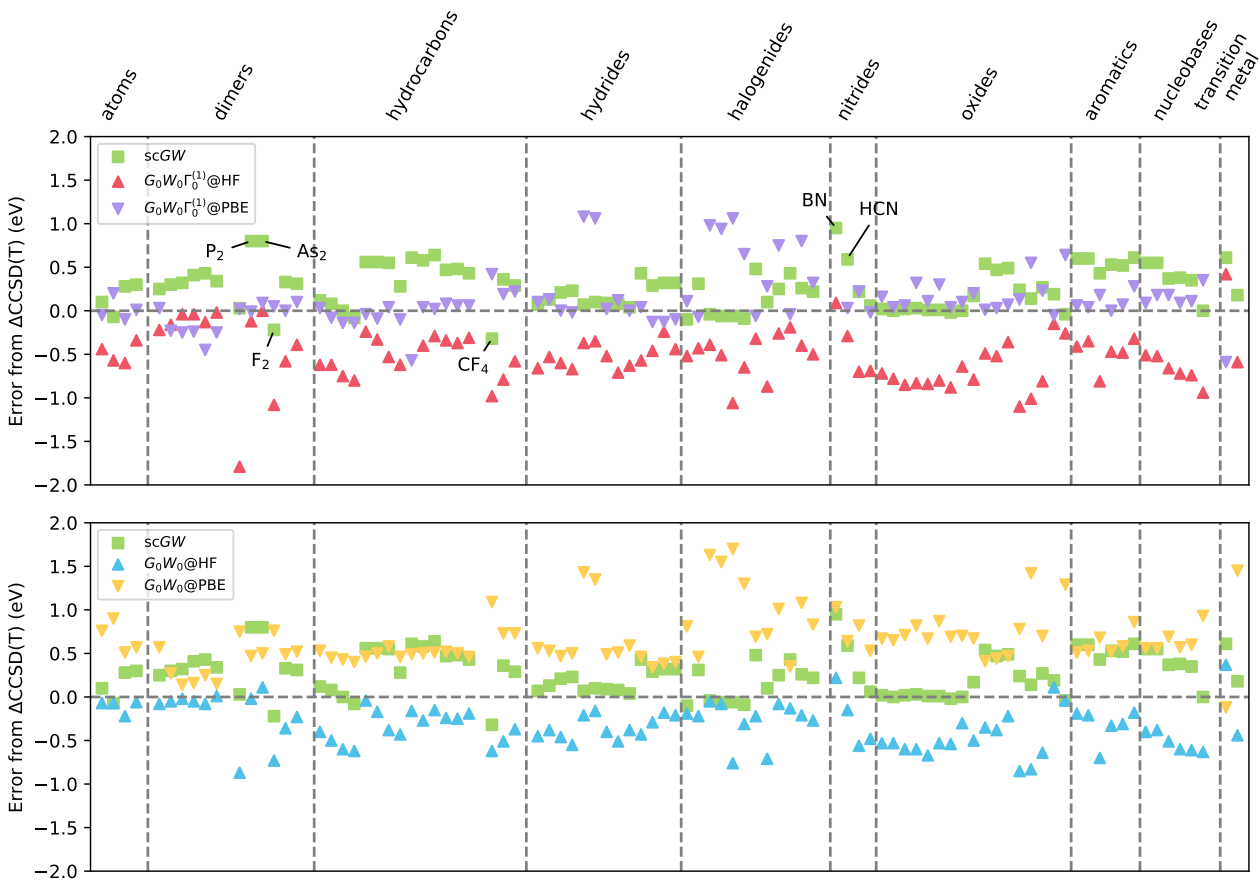


Figure 3: Signed errors from $\Delta\text{CCSD(T)}$ benchmarks, of G_0W_0 , scGW , and $G_0W_0\Gamma_0^{(1)}$ ³³ for the GW100 data set. Some outliers (within their own group) are labeled. Top panel: performances of scGW and $G_0W_0\Gamma_0^{(1)}$ with different starting mean-field calculations. Bottom panel: performance of scGW and G_0W_0 with different starting mean-field calculations.

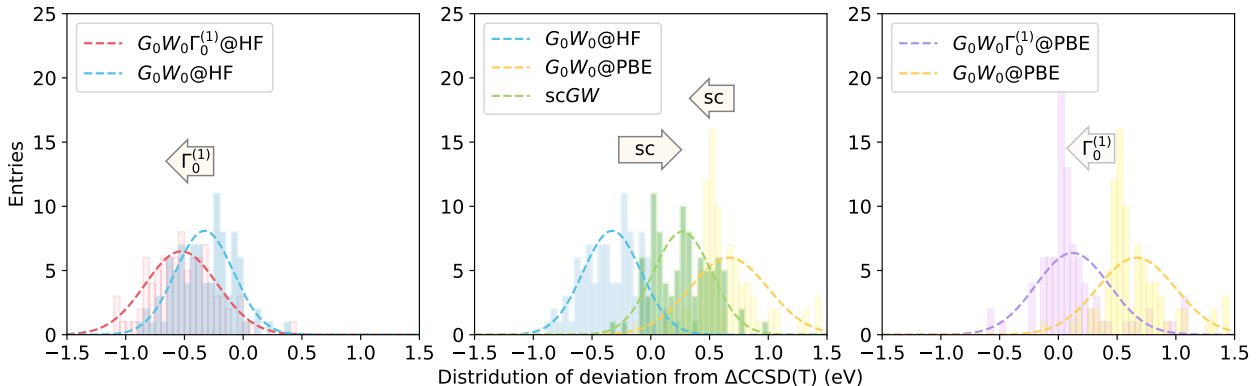


Figure 4: Signed errors from $\Delta\text{CCSD(T)}$ benchmarks, of G_0W_0 , scGW , and $G_0W_0\Gamma_0^{(1)33}$ for the $GW100$ data set. Dashed curves are fitted Gaussian distributions. Left and right panels: influence of $\Gamma_0^{(1)}$ correction on one-shot GW results with different starting mean-field calculations. Middle panel: improvement introduced by self-consistency upon one-shot GW results.

the MAE comparable to scGW .

The effects of different starting points, PBE and HF, on $\Gamma_0^{(1)}$ are analyzed in Fig. 4, where we look at the trends in the error distribution curves for G_0W_0 , $G_0W_0\Gamma_0^{(1)}$, and scGW . Regardless of the initial starting point used for G_0W_0 , the vertex correction $\Gamma_0^{(1)}$ systematically enlarges the value of the first IP peak by a similar amount. Because $G_0W_0@PBE$ generally gives smaller IPs than $\Delta\text{CCSD(T)}$ results, the uniform shift introduced by adding the vertex improves the accuracy of $G_0W_0\Gamma_0^{(1)}@PBE$. For $G_0W_0@HF$, the IPs are already more accurate than those in $G_0W_0@PBE$. Consequently, adding vertex correction leads to diminished accuracy. Based on this observation, we argue that the improvement of $\Gamma_0^{(1)}$ upon G_0W_0 is serendipitous and the accuracy of the overall result that includes vertex correction is mostly dictated by the starting point dependence. Similar mean-field reference dependence of the vertex corrected results has been observed for IPs of molecules containing transition metals.¹⁰⁵ In scGW , such a starting point dependence is effectively removed via the convergence of self-consistent loops.

In Table. 1, we present statistical criteria for the data presented in Fig. 3. We find that $G_0W_0\Gamma_0^{(1)}@PBE$ gives lower MAE than scGW when compared with $\Delta\text{CCSD(T)}$ benchmarks.

Even though *scGW* does not produce the best MAE out of all cases analyzed, one could still argue that it is more reliable to make predictions with the self-consistent scheme, because even with the pre-existing knowledge about the performance of G_0W_0 on a given system, it will still be difficult to know if $\Gamma_0^{(1)}$ would make improvement for such a system or not.

Table 1: MAE in eV for G_0W_0 , $G_0W_0\Gamma_0^{(1)}$, and *scGW* with $\Delta\text{CCSD(T)}$ as benchmarks for the *GW100* data set. The fluctuation in the bracket after each MAE value is the standard deviation of absolute errors. See Table SII in Supporting Information for detailed IP values for each molecule. *Calculated with data reported in Ref. ³³

	G_0W_0	$G_0W_0\Gamma_0^{(1)*}$	<i>scGW</i>
@PBE	0.62(± 0.29)	0.20(± 0.26)	0.29(± 0.22)
@HF	0.35(± 0.23)	0.54(± 0.29)	

Table 2: MAE in eV for $G_0W_0@HF$, *scGW*, $G_0W_0\Gamma^{(NL)}$, and $\Delta\text{CCSD(T)}$ methods for the 29-molecule data set, compared with experimental benchmarks. The fluctuation in the bracket after each MAE value is the standard deviation of absolute errors. See Table SIII in Supporting Information for detailed IP values for each molecule and the cited literature for experimental data. *Calculated with data reported in Ref. ³²

	$G_0W_0@HF$	$G_0W_0\Gamma^{(NL)}@HF$	<i>scGW</i>	$\Delta\text{CCSD(T)}^*$
cc-pVQZ	0.65 (± 0.36)		0.30 (± 0.27)	0.23 (± 0.32)
cc basis limit	0.88 (± 0.38)		0.29 (± 0.26)	
finite PW*	0.42 (± 0.37)	0.37 (± 0.32)		
PW basis limit*	0.69 (± 0.40)	0.46 (± 0.41)		

Comparison of *scGW* and $G_0W_0\Gamma$ with non-local vertex corrections for first IP peaks

Maggio *et al.* calculated first IP peaks for 29 molecules using their non-local vertex correction $\Gamma^{(NL)}$ on top of G_0W_0 in the plane wave (PW) basis. ³² Their first IP results were extrapolated to the PW basis set limit. Here, we compare our *scGW* and their $G_0W_0\Gamma^{(NL)}$ for the first IP prediction against the experimental benchmarks (see Supporting Information Table SIII). Note that while theoretical calculations assume vertical ionizations, this is not necessarily the case in experiments, where vibronic effects might apply. Our G_0W_0 and *scGW* calculations are

performed starting from HF/cc-pVXZ ($X = Q$ and 5) and then extrapolated to the complete basis-set limit. While we cannot compare these results in a very direct manner since they are performed in different bases, we note that the PW basis and cc basis results behave similarly both in accuracy and basis set convergence trend, when compared against experimental benchmarks. This is also confirmed by Maggio *et al.* that GTO basis (cc-pVQZ) produced minimal numerical difference (about 100 meV) from finite PW results computed with the same GW implementation.³²

In Table 2, for the first IPs, we summarize the overall MAE and standard deviation obtained using G_0W_0 and sc GW and compare it against $G_0W_0\Gamma^{(NL)}$ and $\Delta\text{CCSD(T)}$ results from Ref.³² Corresponding numerical data is presented in Table SIII of SI. We observe that by extrapolating G_0W_0 and $G_0W_0\Gamma^{(NL)}$ results from a finite bases to their respective limits, the accuracy deteriorates even though higher number of orbitals are included. For cc basis sets, the MAE for our G_0W_0 increases from 0.65 eV (cc-pVQZ) to 0.88 eV (cc basis limit). Similarly, for the results in plane wave basis,³² the MAE of G_0W_0 increases from 0.42 eV (finite plane wave) to 0.69 eV (plane wave basis limit), and the MAE of $G_0W_0\Gamma^{(NL)}$ increases from 0.37 eV (finite plane wave) to 0.46 eV (plane wave basis limit). In Ref.,³² the extrapolated $G_0W_0\Gamma^{(NL)}$ results were also coupled with convergence issue for some molecules (lithium dimer, phosphorus dimer, and sulfur dioxide). On the other hand sc GW results are essentially converged already at the cc-pVQZ level. As a result, for sc GW , cc-pVQZ results and cc basis limit results are close for most entries (see Supporting Information Table SIII).

Table 2 shows that in the CBS limit for plane waves, vertex correction reduces the MAE for the IPs from 0.69 eV in G_0W_0 to 0.46 eV. Meanwhile, in the CBS limit for the cc basis set family, self-consistency improves the MAE from 0.88 eV at the G_0W_0 level to 0.29 eV.

The magnitude of improvement induced by both self-consistency and vertex correction is illustrated in Fig. 5. In the top panel of Fig. 5, we observe that self-consistency in most cases brings the IP values closer to experiment in comparison to G_0W_0 . The bottom panel shows the magnitude of the improvement brought by vertex correction on top of G_0W_0 , which is

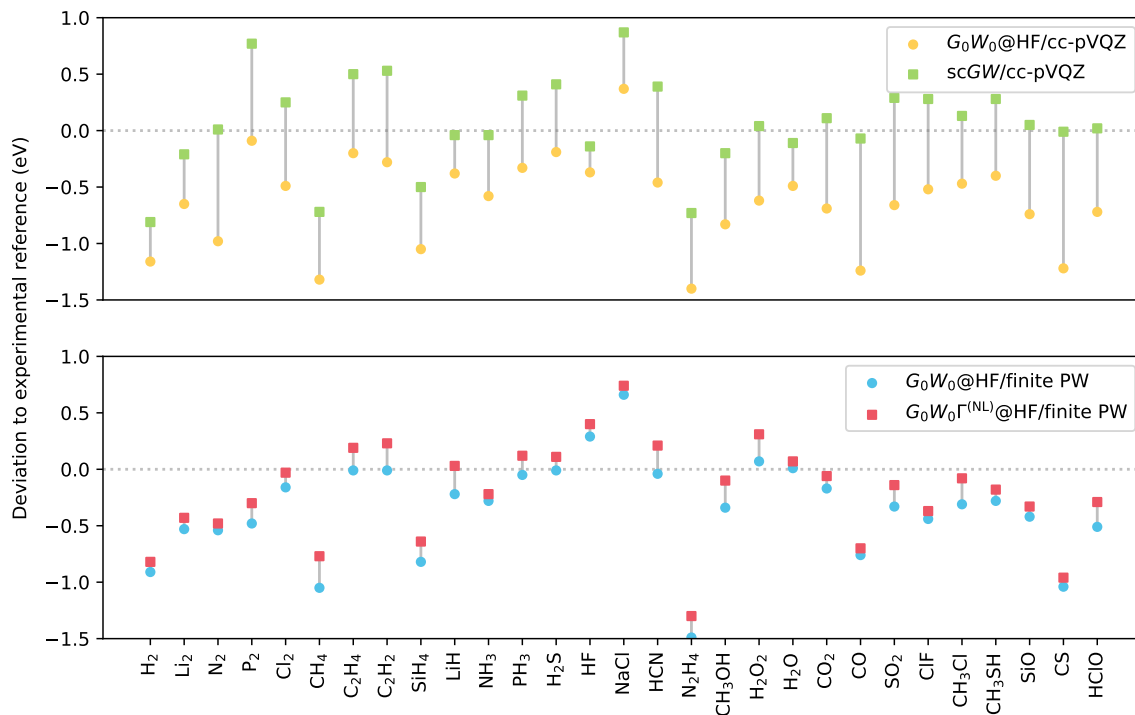


Figure 5: Signed errors from the experimental data, of $G_0W_0@HF$, $scGW$, and $G_0W_0\Gamma^{(NL)}$ for the 29-molecule data set. Top panel: improvement brought upon G_0W_0 prediction by self-consistency in a finite cc basis. Bottom panel: improvement brought by the vertex correction on top of G_0W_0 in a finite plane wave basis, calculated with data reported in Ref. ³²

only minor. Thus, its final accuracy largely depends on a good mean-field starting point of the G_0W_0 calculations.

Overall, we conclude that in the molecular IP domain, improvements introduced by self-consistency is similar to, if not better than, that of vertex corrected G_0W_0 . Moreover, the smaller standard deviation in scGW implies more uniformity in the quality of results. This, combined with the lack of dependence on the starting mean-field solution, makes scGW more favorable.

Conclusion

In this work, we demonstrated the performance of our finite temperature scGW methodology in predicting molecular valence shell IPs. In our implementation, there are no approximations other than (a) density fitting approximation for integral generation; and (b) the Nevanlinna analytical continuation employed to obtain spectral data from the converged Green’s function evaluated on the imaginary axis.

Based on our calculations, performing the self-consistency generally improves upon G_0W_0 results and leads to convergence of calculations with different mean-field starting points. This eliminates the ambiguity associated with the selecting a mean-field calculation used as the reference for the GW method. The reliability of our scGW method is verified both for the first IPs as well as the inner valence shell IPs, when examined against both theoretical and experimental benchmarks.

For molecular systems, we presented comparisons of our scGW with another post-GW methodology – vertex corrected G_0W_0 – motivated by completing the suite of Hedin’s equations. When comparing different $G_0W_0\Gamma$ variants against scGW, we observed that scGW consistently displays either better or comparable accuracy. The $G_0W_0\Gamma$ results were affected by a strong starting point dependence (inherited from G_0W_0) and the magnitude of error caused by starting points is frequently larger than the correction introduced by the vertex.

Similar dependence was also observed in vertex correction upon polarizability exclusively.⁴⁵

Even though there are scattered cases where $G_0W_0\Gamma$ based on a DFT reference outperforms scGW, full self-consistency is cheaper than evaluating full vertex corrections and gives unbiased results independent of the starting point. Moreover, within the scGW framework, the evaluation of total energies and, consequently, energy differences is possible.^{40,106–108} In contrast, in the G_0W_0 schemes, the energy is ill defined since its value strongly depends on the underlying reference. Additionally, the self-consistency in scGW causes relaxation of the orbitals in the presence of correlation resulting in improved quantities such as the electron density.^{40,42,109}

Moreover, choosing an appropriate type of vertex correction can be a difficult task. In this work, we analyzed three different versions of vertex corrections each employing different approximations and we concluded that it is hard to establish *a priori* which type of vertex correction should be used for a certain problem.

While scGW is generally accurate for the first IP as well as the inner valence shell excitations, depiction of excitations with MQP character is believed to be relatively difficult due to their correlation effects. Nevertheless, at least for the examples analyzed in the Results section, it appears that scGW is capable of not only capturing the qualitative emergence of MQP features but also yielding reasonably accurate excitation energies in this regime. This is particularly advantageous in comparison to methods such as EOM-CCSD, where the presence of satellites may lead to issues with converging the quasiparticle energies.

In summary, vertex correction is generally considered as a preferred way to improve the quality of G_0W_0 results. However, we find that at least for molecules, scGW, without vertex, already provides results that are competitive with the best $G_0W_0\Gamma$ results analyzed here. This, combined with the fact that scGW is essentially a black-box method, makes self-consistency a better route to make improvements upon G_0W_0 .

In the future, one still may want to add additional diagrammatic terms beyond scGW. The best way of doing it, however, is an active field of research. Ideally, the implementation

of vertex corrections should be done based on the self-consistent GW approach where the starting point dependence is removed. Only then the approximations introduced in the formulation of GWT can be meaningfully validated. The self-consistent evaluation of Hedin's equations with an addition of the vertex may become numerically difficult and may result in the appearance of unphysical features such as negative spectral functions.¹¹⁰ When applied within the self-consistent GW scheme, the vertex correction is responsible only for bringing the correlation that is missing in the parent $scGW$ approach, and it does not need to remedy for the lack of the orbital optimization that is present in G_0W_0 . This direction will be explored in our future work.

Acknowledgement

M.W., G.H., V.A., A.S., K.B.W. and D.Z. are supported by the U.S. Department of Energy, Office of Science, Office of Advanced Scientific Computing Research and Office of Basic Energy Sciences, Scientific Discovery through Advanced Computing (SciDAC) program under Award Number DE-SC0022198.

Supporting Information Available

Detailed ionization potential values, spectral functions, and additional comparisons between $scGW$ and G_0W_0 .

References

- (1) Čížek, J. On the Correlation Problem in Atomic and Molecular Systems. Calculation of Wavefunction Components in Ursell-Type Expansion Using Quantum-Field Theoretical Methods. *J. Chem. Phys.* **1966**, *45*, 4256–4266.

- (2) Paldus, J.; Čížek, J.; Shavitt, I. Correlation Problems in Atomic and Molecular Systems. IV. Extended Coupled-Pair Many-Electron Theory and Its Application to the BH_3 Molecule. *Phys. Rev. A* **1972**, *5*, 50–67.
- (3) Bartlett, R. J.; Musiał, M. Coupled-Cluster Theory in Quantum Chemistry. *Rev. Mod. Phys.* **2007**, *79*, 291–352.
- (4) Grüneis, A. In *Handbook of Materials Modeling: Methods: Theory and Modeling*; Andreoni, W., Yip, S., Eds.; Springer International Publishing: Cham, 2020; pp 453–468.
- (5) Schäfer, T.; Libisch, F.; Kresse, G.; Grüneis, A. Local Embedding of Coupled Cluster Theory into the Random Phase Approximation Using Plane Waves. *J. Chem. Phys.* **2021**, *154*, 011101.
- (6) Shi, B. X.; Zen, A.; Kapil, V.; Nagy, P. R.; Grüneis, A.; Michaelides, A. Many-Body Methods for Surface Chemistry Come of Age: Achieving Consensus with Experiments. *J. Am. Chem. Soc.* **2023**, *145*, 25372–25381.
- (7) Foster, J. M.; Boys, S. F. Canonical Configurational Interaction Procedure. *Rev. Mod. Phys.* **1960**, *32*, 300–302.
- (8) Siegbahn, P. E. M. Direct Configuration Interaction with a Reference State Composed of Many Reference Configurations. *Int. J. Quantum Chem.* **1980**, *18*, 1229–1242.
- (9) David Sherrill, C.; Schaefer, H. F. In *Advances in Quantum Chemistry*; Löwdin, P.-O., Sabin, J. R., Zerner, M. C., Brändas, E., Eds.; Academic Press, 1999; Vol. 34; pp 143–269.
- (10) Hohenberg, P.; Kohn, W. Inhomogeneous Electron Gas. *Phys. Rev.* **1964**, *136*, B864–B871.

- (11) Kohn, W.; Sham, L. J. Self-Consistent Equations Including Exchange and Correlation Effects. *Phys. Rev.* **1965**, *140*, A1133–A1138.
- (12) Fetter, A. L.; Walecka, J. D. *Quantum Theory of Many-Particle Systems*; Courier Corporation, 2012.
- (13) Hedin, L. New Method for Calculating the One-Particle Green’s Function with Application to the Electron-Gas Problem. *Phys. Rev.* **1965**, *139*, A796–A823.
- (14) Pickett, W. E.; Wang, C. S. Local-Density Approximation for Dynamical Correlation Corrections to Single-Particle Excitations in Insulators. *Phys. Rev. B* **1984**, *30*, 4719–4733.
- (15) Hybertsen, M. S.; Louie, S. G. Electron Correlation in Semiconductors and Insulators: Band Gaps and Quasiparticle Energies. *Phys. Rev. B* **1986**, *34*, 5390–5413.
- (16) Aryasetiawan, F.; Gunnarsson, O. The *GW* Method. *Rep. Prog. Phys.* **1998**, *61*, 237.
- (17) Stan, A.; Dahlen, N. E.; van Leeuwen, R. Fully Self-Consistent *GW* Calculations for Atoms and Molecules. *EPL* **2006**, *76*, 298.
- (18) Koval, P.; Foerster, D.; Sánchez-Portal, D. Fully Self-Consistent *GW* and Quasiparticle Self-Consistent *GW* for Molecules. *Phys. Rev. B* **2014**, *89*, 155417.
- (19) Kutepov, A.; Savrasov, S. Y.; Kotliar, G. Ground-State Properties of Simple Elements from *GW* Calculations. *Phys. Rev. B* **2009**, *80*, 041103(R).
- (20) Caruso, F.; Dauth, M.; van Setten, M. J.; Rinke, P. Benchmark of *GW* Approaches for the *GW100* Test Set. *J. Chem. Theory Comput.* **2016**, *12*, 5076–5087.
- (21) Holm, B.; von Barth, U. Fully Self-Consistent *GW* Self-Energy of the Electron Gas. *Phys. Rev. B* **1998**, *57*, 2108–2117.

- (22) van Schilfgaarde, M.; Kotani, T.; Faleev, S. Quasiparticle Self-Consistent GW Theory. *Phys. Rev. Lett.* **2006**, *96*, 226402.
- (23) Golze, D.; Dvorak, M.; Rinke, P. The GW Compendium: A Practical Guide to Theoretical Photoemission Spectroscopy. *Front. Chem.* **2019**, *7*.
- (24) Holleboom, L. J.; Snijders, J. G. A Comparison between the Möller–Plesset and Green’s Function Perturbative Approaches to the Calculation of the Correlation Energy in the Many-Electron Problem. *J. Chem. Phys.* **1990**, *93*, 5826–5837.
- (25) Dahlen, N. E.; van Leeuwen, R. Self-Consistent Solution of the Dyson Equation for Atoms and Molecules within a Conserving Approximation. *J. Chem. Phys.* **2005**, *122*, 164102.
- (26) Phillips, J. J.; Zgid, D. Communication: The Description of Strong Correlation within Self-Consistent Green’s Function Second-Order Perturbation Theory. *J. Chem. Phys.* **2014**, *140*, 241101.
- (27) Welden, A. R.; Rusakov, A. A.; Zgid, D. Exploring Connections between Statistical Mechanics and Green’s Functions for Realistic Systems: Temperature Dependent Electronic Entropy and Internal Energy from a Self-Consistent Second-Order Green’s Function. *J. Chem. Phys.* **2016**, *145*, 204106.
- (28) Iskakov, S.; Rusakov, A. A.; Zgid, D.; Gull, E. Effect of Propagator Renormalization on the Band Gap of Insulating Solids. *Phys. Rev. B* **2019**, *100*, 085112.
- (29) Schindlmayr, A.; Godby, R. W. Systematic Vertex Corrections through Iterative Solution of Hedin’s Equations Beyond the *GW* Approximation. *Phys. Rev. Lett.* **1998**, *80*, 1702–1705.
- (30) Romaniello, P.; Guyot, S.; Reining, L. The Self-Energy beyond *GW*: Local and Non-local Vertex Corrections. *J. Chem. Phys.* **2009**, *131*, 154111.

- (31) Romaniello, P.; Bechstedt, F.; Reining, L. Beyond the GW approximation: Combining correlation channels. *Phys. Rev. B* **2012**, *85*, 155131.
- (32) Maggio, E.; Kresse, G. GW Vertex Corrected Calculations for Molecular Systems. *J. Chem. Theory Comput.* **2017**, *13*, 4765–4778.
- (33) Wang, Y.; Rinke, P.; Ren, X. Assessing the $G_0W_0\Gamma_0^{(1)}$ Approach: Beyond G_0W_0 with Hedin’s Full Second-Order Self-Energy Contribution. *J. Chem. Theory Comput.* **2021**, *17*, 5140–5154.
- (34) Ren, X.; Marom, N.; Caruso, F.; Scheffler, M.; Rinke, P. Beyond the GW approximation: A second-order screened exchange correction. *Phys. Rev. B* **2015**, *92*, 081104.
- (35) Grüneis, A.; Kresse, G.; Hinuma, Y.; Oba, F. Ionization Potentials of Solids: The Importance of Vertex Corrections. *Phys. Rev. Lett.* **2014**, *112*, 096401.
- (36) Kutepov, A. L. Electronic Structure of Na, K, Si, and LiF from Self-Consistent Solution of Hedin’s Equations Including Vertex Corrections. *Phys. Rev. B* **2016**, *94*, 155101.
- (37) Kutepov, A. L. Self-Consistent Solution of Hedin’s Equations: Semiconductors and Insulators. *Phys. Rev. B* **2017**, *95*, 195120.
- (38) Iskakov, S.; Yeh, C.-N.; Gull, E.; Zgid, D. Ab Initio Self-Energy Embedding for the Photoemission Spectra of NiO and MnO. *Phys. Rev. B* **2020**, *102*, 085105.
- (39) Yeh, C.-N.; Iskakov, S.; Zgid, D.; Gull, E. Fully Self-Consistent Finite-Temperature GW in Gaussian Bloch Orbitals for Solids. *Phys. Rev. B* **2022**, *106*, 235104.
- (40) Caruso, F.; Rinke, P.; Ren, X.; Rubio, A.; Scheffler, M. Self-Consistent GW : All-electron Implementation with Localized Basis Functions. *Phys. Rev. B* **2013**, *88*, 075105.

- (41) Shishkin, M.; Marsman, M.; Kresse, G. Accurate Quasiparticle Spectra from Self-Consistent GW Calculations with Vertex Corrections. *Phys. Rev. Lett.* **2007**, *99*, 246403.
- (42) Caruso, F.; Rinke, P.; Ren, X.; Scheffler, M.; Rubio, A. Unified Description of Ground and Excited States of Finite Systems: The Self-Consistent GW Approach. *Phys. Rev. B* **2012**, *86*, 081102.
- (43) Yeh, C.-N.; Shee, A.; Sun, Q.; Gull, E.; Zgid, D. Relativistic Self-Consistent GW: Exact Two-Component Formalism with One-Electron Approximation for Solids. *Phys. Rev. B* **2022**, *106*, 085121.
- (44) Förster, A.; van Lenthe, E.; Spadetto, E.; Visscher, L. Two-Component GW Calculations: Cubic Scaling Implementation and Comparison of Vertex-Corrected and Partially Self-Consistent GW Variants. *J. Chem. Theory Comput.* **2023**, *19*, 5958–5976.
- (45) Lewis, A. M.; Berkelbach, T. C. Vertex Corrections to the Polarizability Do Not Improve the GW Approximation for the Ionization Potential of Molecules. *J. Chem. Theory Comput.* **2019**, *15*, 2925–2932.
- (46) Förster, A.; Visscher, L. Exploring the Statically Screened G3W2 Correction to the GW Self-Energy: Charged Excitations and Total Energies of Finite Systems. *Phys. Rev. B* **2022**, *105*, 125121.
- (47) Mejuto-Zaera, C.; Weng, G.; Romanova, M.; Cotton, S. J.; Whaley, K. B.; Tubman, N. M.; Vlček, V. Are Multi-Quasiparticle Interactions Important in Molecular Ionization? *J. Chem. Phys.* **2021**, *154*, 121101.
- (48) Takada, Y. Inclusion of Vertex Corrections in the Self-Consistent Calculation of Quasiparticles in Metals. *Phys. Rev. Lett.* **2001**, *87*, 226402.

- (49) Minnhagen, P. Vertex Correction Calculations for an Electron Gas. *J. Phys. C: Solid State Phys.* **1974**, *7*, 3013.
- (50) Onida, G.; Reining, L.; Rubio, A. Electronic Excitations: Density-functional versus Many-Body Green's-Function Approaches. *Rev. Mod. Phys.* **2002**, *74*, 601–659.
- (51) Lan, T. N.; Shee, A.; Li, J.; Gull, E.; Zgid, D. Testing Self-Energy Embedding Theory in Combination with GW. *Phys. Rev. B* **2017**, *96*, 155106.
- (52) Yeh, C.-N.; Iskakov, S.; Zgid, D.; Gull, E. Electron Correlations in the Cubic Paramagnetic Perovskite Sr(V,Mn)O₃: Results from Fully Self-Consistent Self-Energy Embedding Calculations. *Phys. Rev. B* **2021**, *103*, 195149.
- (53) Kananenka, A. A.; Welden, A. R.; Lan, T. N.; Gull, E.; Zgid, D. Efficient Temperature-Dependent Green's Function Methods for Realistic Systems: Using Cubic Spline Interpolation to Approximate Matsubara Green's Functions. *J. Chem. Theory Comput.* **2016**, *12*, 2250–2259.
- (54) Gull, E.; Iskakov, S.; Krivenko, I.; Rusakov, A. A.; Zgid, D. Chebyshev Polynomial Representation of Imaginary-Time Response Functions. *Phys. Rev. B* **2018**, *98*, 075127.
- (55) Dong, X.; Zgid, D.; Gull, E.; Strand, H. U. R. Legendre-Spectral Dyson Equation Solver with Super-Exponential Convergence. 2020.
- (56) Li, J.; Wallerberger, M.; Chikano, N.; Yeh, C.-N.; Gull, E.; Shinaoka, H. Sparse Sampling Approach to Efficient Ab Initio Calculations at Finite Temperature. *Phys. Rev. B* **2020**, *101*, 035144.
- (57) Dunlap, B. I. Robust and Variational Fitting. *Phys. Chem. Chem. Phys.* **2000**, *2*, 2113–2116.

- (58) Fei, J.; Yeh, C.-N.; Gull, E. Nevanlinna Analytical Continuation. *Phys. Rev. Lett.* **2021**, *126*, 056402.
- (59) Huang, Z.; Gull, E.; Lin, L. Robust Analytic Continuation of Green's Functions via Projection, Pole Estimation, and Semidefinite Relaxation. *Phys. Rev. B* **2023**, *107*, 075151.
- (60) Faleev, S. V.; van Schilfgaarde, M.; Kotani, T. All-Electron Self-Consistent GW Approximation: Application to Si, MnO, and NiO. *Phys. Rev. Lett.* **2004**, *93*, 126406.
- (61) Shishkin, M.; Kresse, G. Self-Consistent GW Calculations for Semiconductors and Insulators. *Phys. Rev. B* **2007**, *75*, 235102.
- (62) van Schilfgaarde, M.; Kotani, T.; Faleev, S. Quasiparticle Self-Consistent GW Theory. *Phys. Rev. Lett.* **2006**, *96*, 226402.
- (63) Cao, H.; Yu, Z.; Lu, P.; Wang, L.-W. Fully Converged Plane-Wave-Based Self-Consistent GW Calculations of Periodic Solids. *Phys. Rev. B* **2017**, *95*, 035139.
- (64) Del Sole, R.; Reining, L.; Godby, R. W. GW Γ Approximation for Electron Self-Energies in Semiconductors and Insulators. *Phys. Rev. B* **1994**, *49*, 8024–8028.
- (65) Bruneval, F.; Sottile, F.; Olevano, V.; Del Sole, R.; Reining, L. Many-Body Perturbation Theory Using the Density-Functional Concept: Beyond the GW Approximation. *Phys. Rev. Lett.* **2005**, *94*, 186402.
- (66) Morris, A. J.; Stankovski, M.; Delaney, K. T.; Rinke, P.; García-González, P.; Godby, R. W. Vertex Corrections in Localized and Extended Systems. *Phys. Rev. B* **2007**, *76*, 155106.
- (67) Hung, L.; Da Jornada, F. H.; Souto-Casares, J.; Chelikowsky, J. R.; Louie, S. G.; Ögüt, S. Excitation Spectra of Aromatic Molecules within a Real-Space GW -BSE

- Formalism: Role of Self-Consistency and Vertex Corrections. *Phys. Rev. B* **2016**, *94*, 085125.
- (68) Starke, R.; Kresse, G. Self-Consistent Green Function Equations and the Hierarchy of Approximations for the Four-Point Propagator. *Phys. Rev. B* **2012**, *85*, 075119.
- (69) Szabo, A.; Ostlund, N. S. Interaction Energies between Closed-Shell Systems: The Correlation Energy in the Random Phase Approximation. *Int. J. Quantum Chem.* **1977**, *12*, 389–395.
- (70) Colonna, N.; Hellgren, M.; De Gironcoli, S. Molecular Bonding with the RPax: From Weak Dispersion Forces to Strong Correlation. *Phys. Rev. B* **2016**, *93*, 195108.
- (71) Watabe, M. The Influence of Coulomb Correlation on Various Metallic Properties. *Prog. Theor. Phys.* **1963**, *29*, 519–527.
- (72) Vlček, V. Stochastic Vertex Corrections: Linear Scaling Methods for Accurate Quasi-particle Energies. *J. Chem. Theory Comput.* **2019**, *15*, 6254–6266.
- (73) van Setten, M. J.; Caruso, F.; Sharifzadeh, S.; Ren, X.; Scheffler, M.; Liu, F.; Lischner, J.; Lin, L.; Deslippe, J. R.; Louie, S. G.; Yang, C.; Weigend, F.; Neaton, J. B.; Evers, F.; Rinke, P. GW100: Benchmarking G0W0 for Molecular Systems. *J. Chem. Theory Comput.* **2015**, *11*, 5665–5687.
- (74) Knight, J. W.; Wang, X.; Gallandi, L.; Dolgounitcheva, O.; Ren, X.; Ortiz, J. V.; Rinke, P.; Körzdörfer, T.; Marom, N. Accurate Ionization Potentials and Electron Affinities of Acceptor Molecules III: A Benchmark of *GW* Methods. *J. Chem. Theory Comput.* **2016**, *12*, 615–626.
- (75) Curtiss, L. A.; Raghavachari, K.; Redfern, P. C.; Pople, J. A. Assessment of Gaussian-2 and Density Functional Theories for the Computation of Enthalpies of Formation. *J. Chem. Phys.* **1997**, *106*, 1063–1079.

- (76) Haunschuld, R.; Klopper, W. New Accurate Reference Energies for the G2/97 Test Set. *J. Chem. Phys.* **2012**, *136*, 164102.
- (77) Perdew, J. P.; Burke, K.; Ernzerhof, M. Generalized Gradient Approximation Made Simple. *Phys. Rev. Lett.* **1996**, *77*, 3865–3868.
- (78) Helgaker, T.; Klopper, W.; Koch, H.; Noga, J. Basis-Set Convergence of Correlated Calculations on Water. *J. Chem. Phys.* **1997**, *106*, 9639–9646.
- (79) Halkier, A.; Helgaker, T.; Jørgensen, P.; Klopper, W.; Olsen, J. Basis-Set Convergence of the Energy in Molecular Hartree–Fock Calculations. *Chem. Phys. Lett.* **1999**, *302*, 437–446.
- (80) Rangel, T.; Hamed, S. M.; Bruneval, F.; Neaton, J. B. Evaluating the GW Approximation with CCSD(T) for Charged Excitations Across the Oligoacenes. *J. Chem. Theory Comput.* **2016**, *12*, 2834–2842.
- (81) Han, X.-J.; Liao, H.-J.; Xie, H.-D.; Huang, R.-Z.; Meng, Z.-Y.; Xiang, T. Analytic Continuation with Padé Decomposition. *Chinese Phys. Lett.* **2017**, *34*, 077102.
- (82) Sun, Q.; Berkelbach, T. C.; Blunt, N. S.; Booth, G. H.; Guo, S.; Li, Z.; Liu, J.; McClain, J. D.; Sayfutyarova, E. R.; Sharma, S.; Wouters, S.; Chan, G. K.-L. PySCF: The Python-based Simulations of Chemistry Framework. *WIREs Computational Molecular Science* **2018**, *8*, e1340.
- (83) Sun, Q.; Zhang, X.; Banerjee, S.; Bao, P.; Barbry, M.; Blunt, N. S.; Bogdanov, N. A.; Booth, G. H.; Chen, J.; Cui, Z.-H.; Eriksen, J. J.; Gao, Y.; Guo, S.; Hermann, J.; Hermes, M. R.; Koh, K.; Koval, P.; Lehtola, S.; Li, Z.; Liu, J.; Mardirossian, N.; McClain, J. D.; Motta, M.; Mussard, B.; Pham, H. Q.; Pulkin, A.; Purwanto, W.; Robinson, P. J.; Ronca, E.; Sayfutyarova, E. R.; Scheurer, M.; Schurkus, H. F.; Smith, J. E. T.; Sun, C.; Sun, S.-N.; Upadhyay, S.; Wagner, L. K.; Wang, X.; White, A.;

- Whitfield, J. D.; Williamson, M. J.; Wouters, S.; Yang, J.; Yu, J. M.; Zhu, T.; Berkelbach, T. C.; Sharma, S.; Sokolov, A. Y.; Chan, G. K.-L. Recent Developments in the PySCF Program Package. *J. Chem. Phys.* **2020**, *153*, 024109.
- (84) Kendall, R. A.; Dunning, Jr., Thom H.; Harrison, R. J. Electron Affinities of the First-row Atoms Revisited. Systematic Basis Sets and Wave Functions. *J. Chem. Phys.* **1992**, *96*, 6796–6806.
- (85) Woon, D. E.; Dunning, Jr., Thom H. Gaussian Basis Sets for Use in Correlated Molecular Calculations. III. The Atoms Aluminum through Argon. *J. Chem. Phys.* **1993**, *98*, 1358–1371.
- (86) Pritchard, B. P.; Altarawy, D.; Didier, B.; Gibson, T. D.; Windus, T. L. New Basis Set Exchange: An Open, up-to-Date Resource for the Molecular Sciences Community. *J. Chem. Inf. Model.* **2019**, *59*, 4814–4820.
- (87) Tubman, N. M.; Lee, J.; Takeshita, T. Y.; Head-Gordon, M.; Whaley, K. B. A Deterministic Alternative to the Full Configuration Interaction Quantum Monte Carlo Method. *J. Chem. Phys.* **2016**, *145*, 044112.
- (88) Holmes, A. A.; Tubman, N. M.; Umrigar, C. J. Heat-Bath Configuration Interaction: An Efficient Selected Configuration Interaction Algorithm Inspired by Heat-Bath Sampling. *J. Chem. Theory Comput.* **2016**, *12*, 3674–3680.
- (89) Geertsen, J.; Rittby, M.; Bartlett, R. J. The Equation-of-Motion Coupled-Cluster Method: Excitation Energies of Be and CO. *Chem. Phys. Lett.* **1989**, *164*, 57–62.
- (90) Stanton, J. F.; Bartlett, R. J. The Equation of Motion Coupled-Cluster Method. A Systematic Biorthogonal Approach to Molecular Excitation Energies, Transition Probabilities, and Excited State Properties. *J. Chem. Phys.* **1993**, *98*, 7029–7039.

- (91) Krylov, A. I. Equation-of-Motion Coupled-Cluster Methods for Open-Shell and Electronically Excited Species: The Hitchhiker’s Guide to Fock Space. *Annu. Rev. Phys. Chem.* **2008**, *59*, 433–462.
- (92) Musiał, M.; Kucharski, S. A.; Bartlett, R. J. Equation-of-Motion Coupled Cluster Method with Full Inclusion of the Connected Triple Excitations for Ionized States: IP-EOM-CCSDT. *J. Chem. Phys.* **2003**, *118*, 1128–1136.
- (93) Ranasinghe, D. S.; Margraf, J. T.; Perera, A.; Bartlett, R. J. Vertical Valence Ionization Potential Benchmarks from Equation-of-Motion Coupled Cluster Theory and QTP Functionals. *J. Chem. Phys.* **2019**, *150*, 074108.
- (94) Matthews, D. A.; Cheng, L.; Harding, M. E.; Lipparini, F.; Stopkowicz, S.; Jagau, T.-C.; Szalay, P. G.; Gauss, J.; Stanton, J. F. Coupled-cluster techniques for computational chemistry: The CFOUR program package. *J. Chem. Phys.* **2020**, *152*, 214108.
- (95) Scuseria, G. E.; Henderson, T. M.; Bulik, I. W. Particle-Particle and Quasiparticle Random Phase Approximations: Connections to Coupled Cluster Theory. *J. Chem. Phys.* **2013**, *139*, 104113.
- (96) McClain, J.; Lischner, J.; Watson, T.; Matthews, D. A.; Ronca, E.; Louie, S. G.; Berkelbach, T. C.; Chan, G. K.-L. Spectral Functions of the Uniform Electron Gas via Coupled-Cluster Theory and Comparison to the GW and Related Approximations. *Phys. Rev. B* **2016**, *93*, 235139.
- (97) Lange, M. F.; Berkelbach, T. C. On the Relation between Equation-of-Motion Coupled-Cluster Theory and the GW Approximation. *J. Chem. Theory Comput.* **2018**, *14*, 4224–4236.
- (98) Quintero-Monsebaiz, R.; Monino, E.; Marie, A.; Loos, P.-F. Connections between Many-Body Perturbation and Coupled-Cluster Theories. *J. Chem. Phys.* **2022**, *157*, 231102.

- (99) Tölle, J.; Kin-Lic Chan, G. Exact Relationships between the GW Approximation and Equation-of-Motion Coupled-Cluster Theories through the Quasi-Boson Formalism. *J. Chem. Phys.* **2023**, *158*, 124123.
- (100) Cederbaum, L. S.; Domcke, W.; Schirmer, J.; von Niessen, W. Many-Body Effects in Valence and Core Photoionization of Molecules. *Phys. Scr.* **1980**, *21*, 481–491.
- (101) Guzzo, M.; Lani, G.; Sottile, F.; Romaniello, P.; Gatti, M.; Kas, J. J.; Rehr, J. J.; Silly, M. G.; Sirotti, F.; Reining, L. Valence Electron Photoemission Spectrum of Semiconductors: *Ab Initio* Description of Multiple Satellites. *Phys. Rev. Lett.* **2011**, *107*, 166401.
- (102) Katharina Krause, M. E. H.; Klopper, W. Coupled-Cluster Reference Values for the GW27 and GW100 Test Sets for the Assessment of GW Methods. *Mol. Phys.* **2015**, *113*, 1952–1960.
- (103) Förster, A.; Visscher, L. GW100: A Slater-Type Orbital Perspective. *J. Chem. Theory Comput.* **2021**, *17*, 5080–5097.
- (104) Bruneval, F.; Dattani, N.; van Setten, M. J. The GW Miracle in Many-Body Perturbation Theory for the Ionization Potential of Molecules. *Front. Chem.* **2021**, *9*.
- (105) Wang, Y.; Ren, X. Vertex Effects in Describing the Ionization Energies of the First-Row Transition-Metal Monoxide Molecules. *J. Chem. Phys.* **2022**, *157*, 214115.
- (106) Galitskii, V. M.; Migdal, A. B. Application of Quantum Field Theory Methods to the Many Body Problem. *Sov. Phys. JETP* **1958**, *7*, 18.
- (107) Holm, B.; Aryasetiawan, F. Total Energy from the Galitskii-Migdal Formula Using Realistic Spectral Functions. *Phys. Rev. B* **2000**, *62*, 4858–4865.
- (108) Stan, A.; Dahlen, N. E.; van Leeuwen, R. Levels of Self-Consistency in the GW Approximation. *J. Chem. Phys.* **2009**, *130*, 114105.

- (109) Caruso, F.; Rinke, P.; Ren, X.; Rubio, A.; Scheffler, M. Self-Consistent \$GW\$: All-electron Implementation with Localized Basis Functions. *Phys. Rev. B* **2013**, *88*, 075105.
- (110) Pavlyukh, Y.; Stefanucci, G.; van Leeuwen, R. Dynamically Screened Vertex Correction to GW. *Phys. Rev. B* **2020**, *102*, 045121.

Supporting Information:

Comparing self-consistent GW and vertex corrected G_0W_0 ($G_0W_0\Gamma$) accuracy for molecular ionization potentials

Ming Wen,[†] Vibin Abraham,[†] Gaurav Harsha,[†] Avijit Shee,[‡] K. Birgitta Whaley,[‡] and Dominika Zgid^{*,†,¶}

[†]*Department of Chemistry, University of Michigan, Ann Arbor, Michigan 48109*

[‡]*Department of Chemistry, University of California, Berkeley, California 94720-1460*

[¶]*Department of Physics, University of Michigan, Ann Arbor, Michigan 48109*

E-mail: zgid.umich@edu

A. Inner valence shell ionizations

In Table S1, we report our detailed data for the first and few inner valence ionization peaks for each molecule entry. For ammonia, water, nitrogen, acetylene, and methane, $G_0W_0\Gamma_X$ and ASCI results were reported by Mejuto-Zaera *et. al.*¹ For G_0W_0 , G_0W_0 , *scGW*, and ASCI, results are extrapolated to the aug-cc basis limit. The EOM columns are computed using aug-cc-pVQZ and not extrapolated.

Table S1: First few ionization potential predictions (in eV) for molecules. G_0W_0 , $G_0W_0\Gamma$, and ASCI data cited from Ref.¹ are reproduced in this table with permission, © Copyright 2024 AIP Publishing LLC. *Methane’s G_0W_0 , $G_0W_0\Gamma$, and ASCI results were reported in cc basis. **Unable to converge.

Molecule	Peak	G_0W_0 ¹	$G_0W_0\Gamma_X$ ¹	<i>scGW</i>	EOM-CCSD	EOM-CCSDT	ASCI ¹
Ethylene	1			-10.28	-10.76	-10.72	
	2			-13.20	-13.16	-13.10	
	3			-14.83	-15.01	-14.86	
	4			-16.36	-16.38	-16.20	
Hydrogen fluoride	1-2			-16.39	-16.15	-16.10	
	3			-20.09	-20.06	-20.01	
	4			-39.57	**	**	
Carbon monoxide	1			-14.20	-14.50	-14.15	
	2-3			-15.20	-15.63	-15.57	
	4			-19.64	-19.57	-19.02	
	5			-33.57	**	**	
Ammonia	1	-11.70	-10.85	-11.00	-10.94	-10.93	-10.81
	2-3	-17.12	-16.70	-16.58	-16.65	-16.61	-16.51
	4	-31.08	-27.58	-28.07	-27.90	-26.97	-27.36
Water	1	-13.36	-12.94	-12.84	-12.70	-12.70	-12.75
	2	-15.44	-15.03	-14.99	-14.90	-14.91	-14.90
	3	-19.62	-19.20	-19.02	-19.07	-19.06	-19.10
	4	-35.06	-32.02	-32.91	-32.88	-32.73	-32.99
Nitrogen	1	-17.28	-16.28	-15.69	-15.74	-15.60	-15.54
	2-3	-16.82	-17.11	-16.48	-17.34	-17.05	-17.05
	4	-21.14	-19.62	-19.14	**	-18.98	-18.88
Acetylene	1-2	-11.18	-11.27	-11.05	-11.66	-11.51	-11.45
	3	-18.53	-17.95	-17.25	-17.34	-17.19	-17.15
	4	-20.90	-19.62	-19.32	-19.21	-19.05	-19.05
	5	-28.06	-24.31	-24.65	-24.57	-24.70	-24.13
Methane*	1-3	-14.83	-14.61	-14.39	-14.45	-14.36	-14.35
	4	-25.69	-22.74	-23.43	-23.42	-23.12	-23.25

In Fig. S1 and S2, we present five examples of spectral functions produced from the

scGW/aug-cc-pVQZ calculations via Nevanlinna analytical continuation. Similar spectral functions rendered by stochastic $G_0W_0\Gamma_X$ were reported in Ref.¹ Notice that in ammonia and water we had the complicated multi-peak feature in the MQP regime. We identify the MQP peak by increasing the broadening factor so that the complicated multi-peak feature melted into a singular broad peak, which corresponds to the IP number we report in TABLE S1.

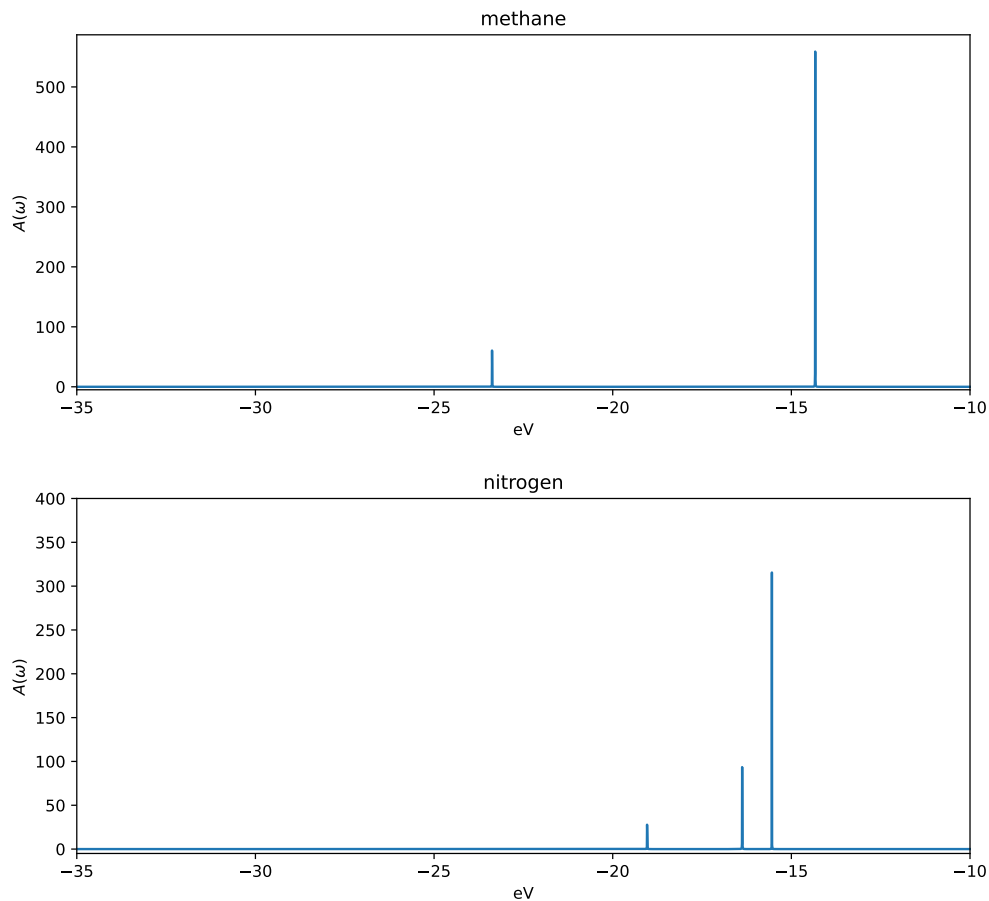


Figure S1: Spectral functions of methane and nitrogen. The spectral functions were produced using the analytically continued data from *scGW* results.

In Fig. S3, we present the absolute deviation when changing the ASCI benchmarks¹ to EOM-CCSDT benchmarks.

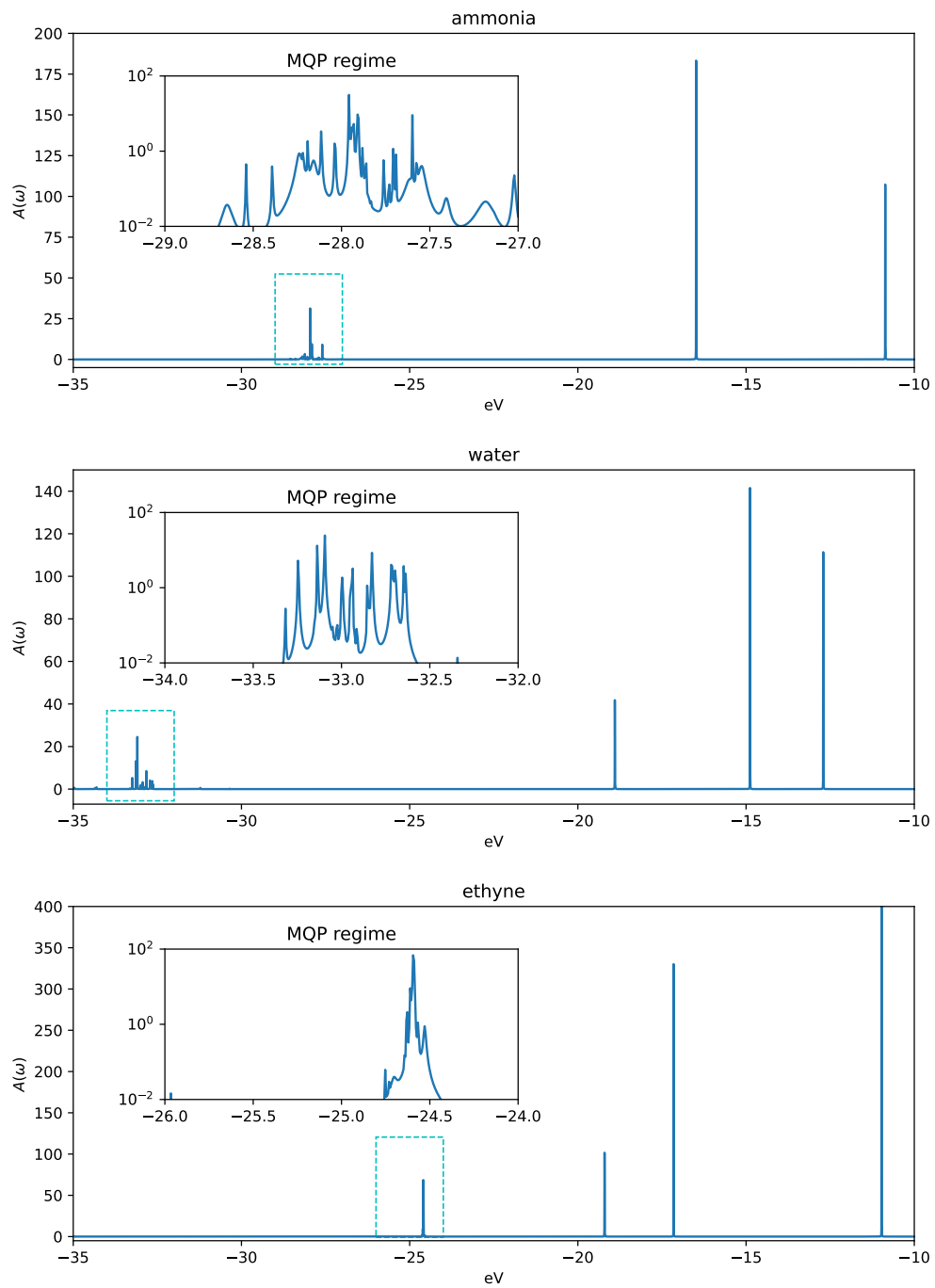


Figure S2: Spectral functions of ammonia, water, and acetylene. The spectral functions were produced using the analytically continued data from *scGW* results. The MQP regimes insets are plotted in algorithmic scale.

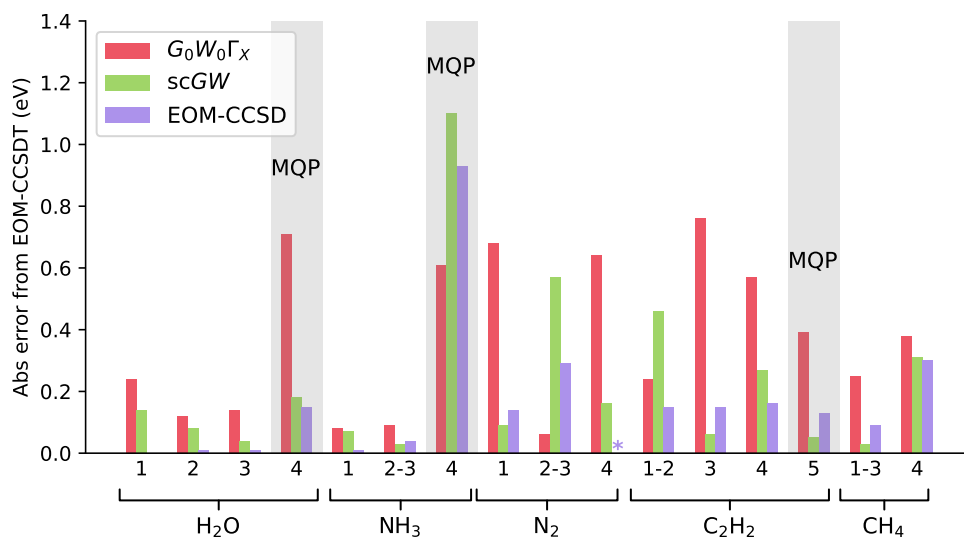


Figure S3: Absolute error of scGW, $G_0W_0\Gamma_X$, and EOM-CCSD predictions of the first and inner shell ionization peaks from the EOM-CCSDT data. *EOM-CCSD calculation did not converge.

B. First ionization peaks

We present our validation test on the $GW100$ set. We compared our $scGW$ method to $G_0W_0\Gamma_0^{(1)}$ by Wang *et al.*² while keeping the level of theory as similar as possible. Initializations for both approaches are done using HF/def2-TZVPP and PBE/def2-TZVPP. Molecules containing elements in the fourth row or beyond are excluded, since the all-electron basis set of def2-TZVPP for these elements was not available. Total of 93 molecules are kept.

Firstly, we need to confirm that finite temperature $scGW$ (on the imaginary axis) and $G_0W_0\Gamma_0^{(1)}$ (on the real axis) can produce the same results after the first iteration, *i.e.* the G_0W_0 level. If so, we can make sure the comparison is appropriate and based on similar theoretical footing. In Fig. S4 the G_0W_0 results for both schemes fit well with no obvious outliers. Additionally, we compared our $scGW$ with past implementation of $scGW$ by Caruso *et al.*³ This observation also supports that one can reliably recover spectral information from the Green's function on imaginary axis via analytical continuation.

Table S2: First ionization potentials (in eV) calculated from $G_0W_0@HF$, $G_0W_0@PBE$, $scGW$, and $\Delta CCSD(T)$ for the $GW100$ set.

Index	Molecule	$G_0W_0@HF$	$G_0W_0@PBE$	$scGW$	$CCSD(T)^4$	Index	Molecule	$G_0W_0@HF$	$G_0W_0@PBE$	$scGW$	$CCSD(T)^4$
1	He	-24.58	-23.75	-24.41	-24.51	53	HCl	-12.81	-12.13	-12.28	-12.59
2	Ne	-21.39	-20.49	-21.39	-21.32	54	LiF	-11.37	-9.77	-11.36	-11.32
3	Ar	-15.76	-15.02	-15.26	-15.54	55	MgF ₂	-13.79	-12.29	-13.77	-13.71
4	Kr	-14.00	-13.37	-13.64	-13.94	56	TiF ₄	-16.17	-13.77	-15.47	-15.41
6	H ₂	-16.48	-15.90	-16.15	-16.40	57	AlF ₃	-15.63	-14.14	-15.41	-15.32
7	Li ₂	-5.32	-5.05	-4.97	-5.27	58	BF	-11.31	-10.43	-10.61	-11.09
8	Na ₂	-4.97	-4.92	-4.63	-4.95	59	SF ₄	-13.30	-11.91	-12.49	-12.59
9	Na ₄	-4.29	-4.11	-3.83	-4.24	60	KBr	-8.21	-7.15	-7.88	-8.13
10	Na ₆	-4.47	-4.25	-3.96	-4.39	61	GaCl	-9.90	-9.42	-9.34	-9.77
11	K ₂	-4.06	-3.94	-3.73	-4.07	62	NaCl	-9.24	-7.90	-8.77	-9.03
13	N ₂	-16.35	-14.74	-15.45	-15.48	63	MgCl ₂	-11.93	-10.84	-11.44	-11.66
14	P ₂	-10.55	-10.05	-9.73	-10.53	65	BN	-11.76	-11.08	-11.03	-11.98
15	As ₂	-9.74	-9.34	-9.05	-9.85	66	HCN	-13.87	-13.00	-13.13	-13.72
16	F ₂	-16.31	-14.83	-15.80	-15.58	67	PN	-12.37	-10.99	-11.59	-11.81
17	Cl ₂	-11.77	-10.90	-11.08	-11.41	68	N ₂ H ₄	-10.17	-9.21	-9.63	-9.69
18	Br ₂	-10.75	-9.98	-10.21	-10.52	69	CH ₂ O	-11.37	-10.17	-10.82	-10.84
20	CH ₄	-14.77	-13.91	-14.25	-14.37	70	CH ₃ OH	-11.57	-10.46	-11.04	-11.04
21	C ₂ H ₆	-13.21	-12.35	-12.63	-12.71	71	EtOH	-11.29	-10.05	-10.67	-10.69
22	C ₃ H ₈	-12.63	-11.66	-12.03	-12.03	72	CH ₃ CHO	-10.81	-9.40	-10.18	-10.21
23	C ₄ H ₁₀	-12.19	-11.23	-11.65	-11.57	73	Et ₂ O	-10.49	-9.21	-9.81	-9.82
24	C ₂ H ₄	-10.71	-10.20	-10.11	-10.67	74	HCOOH	-11.95	-10.59	-11.41	-11.42
25	C ₂ H ₂	-11.59	-10.94	-10.86	-11.42	75	H ₂ O ₂	-12.06	-10.87	-11.54	-11.52
26	C ₄	-11.62	-10.64	-10.69	-11.24	76	H ₂ O	-12.87	-11.94	-12.57	-12.57
27	C ₃ H ₆	-11.30	-10.46	-10.59	-10.87	77	CO ₂	-14.21	-13.07	-13.54	-13.71
28	C ₆ H ₆	-9.52	-8.87	-8.75	-9.36	78	CS ₂	-10.33	-9.55	-9.44	-9.98
29	C ₈ H ₈	-8.67	-7.93	-7.82	-8.40	79	OCS	-11.55	-10.74	-10.70	-11.17
30	C ₅ H ₆	-8.86	-8.23	-8.07	-8.71	80	COSe	-10.69	-10.00	-9.98	-10.47
31	C ₂ H ₃ F	-10.79	-10.02	-10.08	-10.55	81	CO	-15.06	-13.43	-13.97	-14.21
32	C ₂ H ₃ Cl	-10.34	-9.58	-9.61	-10.09	82	O ₃	-13.54	-11.73	-12.57	-12.71
33	C ₂ H ₃ Br	-9.46	-8.83	-8.84	-9.27	83	SO ₂	-12.94	-11.61	-12.03	-12.30
35	CF ₄	-16.85	-15.18	-16.55	-16.23	84	BeO	-9.83	-9.16	-9.75	-9.94
36	CCl ₄	-12.01	-10.77	-11.14	-11.50	85	MgO	-7.95	-7.05	-7.95	-7.91
37	CBr ₄	-10.78	-9.67	-10.12	-10.41	86	C ₆ H ₅ CH ₃	-9.16	-8.49	-8.37	-8.97
39	SiH ₄	-13.25	-12.28	-12.73	-12.80	87	C ₆ H ₅ Et	-9.13	-8.43	-8.32	-8.92
40	GeH ₄	-12.88	-11.99	-12.37	-12.50	88	C ₆ F ₆	-10.63	-9.28	-9.50	-9.93
41	Si ₂ H ₆	-11.11	-10.21	-10.44	-10.65	89	C ₆ H ₅ OH	-9.03	-8.22	-8.17	-8.70
42	Si ₅ H ₁₂	-9.82	-8.81	-9.04	-9.27	90	C ₆ H ₅ NH ₂	-8.35	-7.49	-7.52	-8.04
43	LiH	-8.17	-7.02	-7.89	-7.96	91	C ₅ H ₅ N	-9.91	-8.87	-9.12	-9.73
44	KH	-6.29	-4.81	-6.03	-6.13	92	guanine	-8.44	-7.52	-7.48	-8.03
45	BH ₃	-13.67	-12.84	-13.18	-13.27	93	adenine	-8.71	-7.80	-7.78	-8.33
46	B ₂ H ₆	-12.76	-11.74	-12.17	-12.25	94	cytosine	-9.28	-8.08	-8.40	-8.77
47	NH ₃	-11.19	-10.29	-10.77	-10.81	95	thymine	-9.68	-8.49	-8.70	-9.08
48	HN ₃	-11.11	-10.27	-10.25	-10.68	96	uracil	-10.09	-8.86	-9.13	-9.48
49	PH ₃	-10.81	-10.20	-10.23	-10.52	97	urea	-10.68	-9.18	-10.05	-10.05
50	AsH ₃	-10.58	-10.04	-10.08	-10.40	99	Cu ₂	-7.20	-7.61	-6.96	-7.57
51	H ₂ S	-10.52	-9.92	-9.99	-10.31	100	CuCN	-11.29	-9.80	-10.67	-10.85
52	HF	-16.22	-15.29	-16.13	-16.03		MAE	0.32	0.62	0.29	

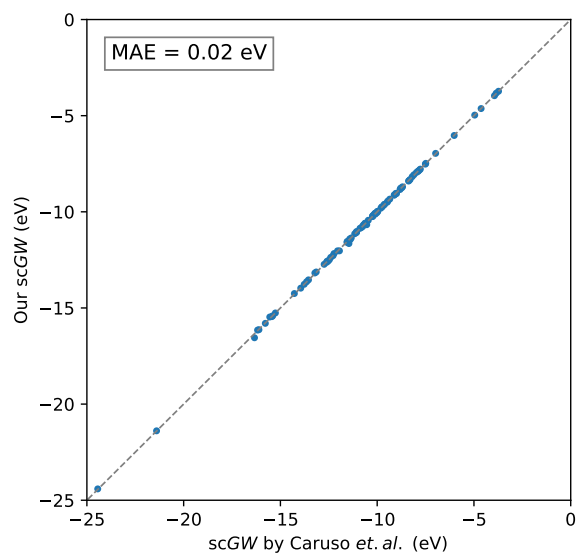
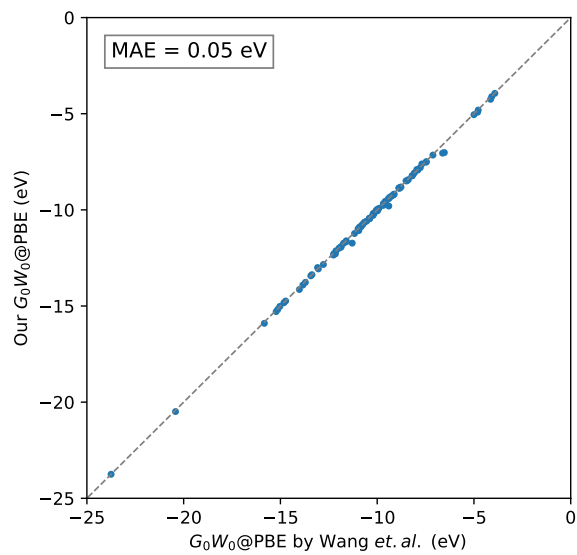


Figure S4: Left: Comparison of ionization potentials derived from G_0W_0 @PBE by Wang *et al.* and our finite temperature version of G_0W_0 @PBE. Right: Comparison of ionization potentials derived from scGW by Caruso *et al.* and our finite temperature version of scGW.

We use HF/cc-pVXZ ($X = Q$ and 5) as the starting point for our subsequent scGW calculations for the 29-molecule data set. Then we compare these results with the vertexed corrected G_0W_0 method ($G_0W_0\Gamma^{(NL)}$ in the main text) proposed by Maggio *et. al.*⁵ Final scGW results are linearly extrapolated to cc basis set limit. The cited data calculated in the plane wave basis were also evaluated with HF starting mean field. Please refer to the original article for their detailed description for energy cut-offs and the extrapolation technique for the PW basis.

Table S3: First ionization potentials (in eV) calculated from CCSD(T), G_0W_0 @HF, scGW, and $G_0W_0\Gamma$ @HF, in cc basis and plane wave basis sets. *Vertical IP values are in italics.

Molecule	cc-pVQZ			cc basis limit		finite PW ⁵		PW basis limit ⁵		Experiment*
	CCSD(T) ⁵	G_0W_0	scGW	G_0W_0	scGW	G_0W_0	$G_0W_0\Gamma$	G_0W_0	$G_0W_0\Gamma$	
hydrogen	-16.39	-16.59	-16.24	-16.65	-16.32	-16.34	-16.25	-16.72	-16.52	-15.43 ⁶
lithium dimer	-5.17	-5.38	-4.94	-5.42	-4.94	-5.26	-5.16	-5.29		-4.73 ⁷
nitrogen	-15.49	-16.56	-15.57	-16.82	-15.66	-16.12	-16.06	-16.56	-16.39	-15.58 ⁸
phosphorus dimer	-10.76	-10.71	-9.85	-11.01	-9.98	-11.10	-10.92	-11.31		-10.62 ⁹
chlorine	-11.62	-11.98	-11.24	-12.35	-11.37	-11.65	-11.52	-12.08	-11.80	<i>-11.49</i> ¹⁰
methane	-14.40	-14.92	-14.32	-15.05	-14.37	-14.65	-14.37	-14.95	-14.57	<i>-13.6</i> ¹¹
ethylene	-10.69	-10.88	-10.18	-11.04	-10.24	-10.69	-10.49	-10.91	-10.66	<i>-10.68</i> ¹¹
acetylene	-11.42	-11.77	-10.96	-11.95	-11.13	-11.50	-11.26	-11.73	-11.43	<i>-11.49</i> ¹¹
silane	-12.82	-13.35	-12.80	-13.50	-12.89	-13.12	-12.94	-13.40	-12.88	<i>-12.3</i> ¹²
lithium hydride	-7.94	-8.28	-7.94	-8.39	-8.02	-8.12	-7.87	-8.26	-7.94	-7.9 ¹³
ammonia	-10.92	-11.40	-10.86	-11.60	-10.98	-11.10	-11.04	-11.45	-11.28	<i>-10.82</i> ¹⁴
phosphine	-10.49	-10.92	-10.28	-11.14	-10.48	-10.64	-10.47	-10.89	-10.66	<i>-10.59</i> ¹⁵
hydrogen sulfide	-10.43	-10.69	-10.09	-10.97	-10.15	-10.51	-10.39	-10.79	-10.60	<i>-10.50</i> ¹⁶
hydrogen fluoride	-16.09	-16.49	-16.26	-16.79	-16.41	-15.83	-15.72	-16.29	-16.18	<i>-16.12</i> ¹⁷
sodium chloride	-9.13	-9.43	-8.93	-9.83	-9.09	-9.14	-9.06	-9.51	-9.32	<i>-9.80</i> ¹⁸
hydrogen cyanide	-13.64	-14.07	-13.22	-14.28	-13.44	-13.65	-13.4	-13.92	-13.61	<i>-13.61</i> ¹⁹
hydrazine	-10.24	-10.38	-9.71	-10.61	-9.83	-10.47	-10.28	-10.86	-10.58	<i>-8.98</i> ²⁰
methanol	-11.08	-11.79	-11.16	-12.03	-11.33	-11.30	-11.06	-11.71	-11.39	<i>-10.96</i> ²¹
hydrogen peroxide	-11.49	-12.32	-11.66	-12.62	-11.91	-11.63	-11.39	-12.12	-11.81	<i>-11.70</i> ²²
water	-12.64	-13.11	-12.73	-13.38	-12.80	-12.61	-12.55	-13.10	-12.92	<i>-12.62</i> ²³
carbon dioxide	-13.78	-14.46	-13.66	-14.78	-13.92	-13.94	-13.83	-14.35	-14.16	<i>-13.77</i> ²⁴
carbon monoxide	-14.05	-15.25	-14.08	-15.47	-14.17	-14.77	-14.71	-15.03	-14.89	<i>-14.01</i> ²⁵
sulfur dioxide	-12.41	-13.16	-12.21	-13.60	-12.48	-12.83	-12.64	-13.20		<i>-12.50</i> ²³
chlorine fluoride	-12.82	-13.29	-12.49	-13.67	-12.73	-13.21	-13.14	-13.49	-13.33	<i>-12.77</i> ¹⁰
chloromethane	-11.41	-11.76	-11.16	-12.10	-11.24	-11.60	-11.37	-11.90	-11.56	<i>-11.29</i> ²³
methanethiol	-9.49	-9.84	-9.16	-10.12	-9.35	-9.72	-9.62	-9.93	-9.76	<i>-9.44</i> ²⁶
silicon monoxide	-11.55	-12.04	-11.25	-12.30	-11.35	-11.72	-11.63	-12.05	-11.78	-11.3 ²⁷
carbon monosulfide	-11.45	-12.55	-11.34	-12.80	-11.44	-12.37	-12.29	-12.63	-12.47	-11.33 ²⁸
hypochlorous acid	-11.30	-11.84	-11.10	-12.20	-11.30	-11.63	-11.41	-11.96	-11.66	-11.12 ²⁹
MAE from experiment	0.23	0.65	0.30	0.88	0.29	0.42	0.37	0.69	0.46	

References

- (1) Mejuto-Zaera, C.; Weng, G.; Romanova, M.; Cotton, S. J.; Whaley, K. B.; Tubman, N. M.; Vlček, V. Are Multi-Quasiparticle Interactions Important in Molecular Ionization? *J. Chem. Phys.* **2021**, *154*, 121101.
- (2) Wang, Y.; Rinke, P.; Ren, X. Assessing the $G_0W_0\Gamma_0^{(1)}$ Approach: Beyond G_0W_0 with Hedin's Full Second-Order Self-Energy Contribution. *J. Chem. Theory Comput.* **2021**, *17*, 5140–5154.
- (3) Caruso, F.; Rinke, P.; Ren, X.; Rubio, A.; Scheffler, M. Self-Consistent GW: All-electron Implementation with Localized Basis Functions. *Phys. Rev. B* **2013**, *88*, 075105.
- (4) Bruneval, F.; Dattani, N.; van Setten, M. J. The GW Miracle in Many-Body Perturbation Theory for the Ionization Potential of Molecules. *Front. Chem.* **2021**, *9*.
- (5) Maggio, E.; Kresse, G. GW Vertex Corrected Calculations for Molecular Systems. *J. Chem. Theory Comput.* **2017**, *13*, 4765–4778.
- (6) McCormack, E.; Gilligan, J. M.; Cornaggia, C.; Eyler, E. E. Measurement of High Rydberg States and the Ionization Potential of H₂. *Phys. Rev. A* **1989**, *39*, 2260–2263.
- (7) Dugourd, Ph.; Rayane, D.; Labastie, P.; Vezin, B.; Chevaleyre, J.; Broyer, M. Measurements of Lithium Cluster Ionization Potentials. *Chem. Phys. Lett.* **1992**, *197*, 433–437.
- (8) Trickl, T.; Cromwell, E. F.; Lee, Y. T.; Kung, A. H. State-selective Ionization of Nitrogen in the $X^2\Sigma_g^+v_+ = 0$ and $v_+ = 1$ States by Two-color (1+1) Photon Excitation near Threshold. *J. Chem. Phys.* **1989**, *91*, 6006–6012.
- (9) K. Bulgin, D.; M. Dyke, J.; Morris, A. HeI Photoelectron Spectrum of the $P_2(X^1\Sigma_g^+)$ Molecule. *J. Chem. Soc., Faraday Trans. 2* **1976**, *72*, 2225–2232.

- (10) Dyke, J. M.; Josland, G. D.; Snijders, J. G.; Boerrigter, P. M. Ionization Energies of the Diatomic Halogens and Interhalogens Studied with Relativistic Hartree-Fock-Slater Calculations. *Chem. Phys.* **1984**, *91*, 419–424.
- (11) Bieri, G.; Åsbrink, L. 30.4-Nm He(II) Photoelectron Spectra of Organic Molecules: Part I. Hydrocarbons. *J. Electron Spectrosc. Relat. Phenom* **1980**, *20*, 149–167.
- (12) Roberge, R.; Sandorfy, C.; Matthews, J. I.; Strausz, O. P. The Far Ultraviolet and HeI Photoelectron Spectra of Alkyl and Fluorine Substituted Silane Derivatives. *J. Chem. Phys.* **1978**, *69*, 5105–5112.
- (13) Lias, S. G.; Levin, R. D.; Kafafi, S. A. *NIST Chemistry WebBook, NIST Standard Reference Database Number 69*; National Institute of Standards and Technology, Eds. Linstrom, P.J. and Mallard W.G. (retrieved Feb. 7, 2024).
- (14) Baumgaertel, H.; Jochims, H. W.; Ruehl, E.; Bock, H.; Dammel, R.; Minkwitz, J.; Nass, R. Photoelectron Spectra and Molecular Properties. 112. Photoelectron and Photoionization Mass Spectra of the Fluoroamines NH₃-nFn. *Inorg. Chem.* **1989**, *28*, 943–949.
- (15) Cowley, A. H.; Kemp, R. A.; Lattman, M.; McKee, M. L. Lewis Base Behavior of Methylated and Fluorinated Phosphines. Photoelectron Spectroscopic Investigation. *Inorg. Chem.* **1982**, *21*, 85–88.
- (16) Bieri, G.; Åsbrink, L.; von Niessen, W. 30.4-Nm He (II) Photoelectron Spectra of Organic Molecules: Part VII. Miscellaneous Compounds. *J. Electron Spectrosc. Relat. Phenom* **1982**, *27*, 129–178.
- (17) Banna, M. S.; Shirley, D. A. Molecular Photoelectron Spectroscopy at 132.3 eV. The Second-Row Hydrides. *J. Chem. Phys.* **1975**, *63*, 4759–4766.
- (18) Potts, A. W.; Price, W. C. Photoelectron Studies of Ionic Materials Using Molecular Beam Techniques. *Phys. Scr.* **1977**, *16*, 191.

- (19) Kreile, J.; Schweig, A.; Theil, W. Experimental and Theoretical Investigation of the Photoionization of Hydrogen Cyanide. *Chem. Phys. Lett.* **1982**, *87*, 473–476.
- (20) Vovna, V. I.; Vilesov, F. I.; Lopatin, S. N. Photoelectron Spectra of Hydrazine and Some Alkyl Derivatives. *Opt. Spectrosc.* **1975**, *38*, 143–144.
- (21) Vorob'ev, A.; Furlei, I.; Sultanov, A.; Khvostenko, V.; Leplyanin, G.; Derzhinskii, A.; Tolstikov, G. Mass Spectrometry of Resonance Capture of Electrons and Photoelectron Spectroscopy of Molecules of Ethylene Oxide, Ethylene Sulfide, and Their Derivatives. *Bull. Acad. Sci. USSR, Div. Chem. Sci.* **1989**, 1388–1394.
- (22) Ashmore, F. S.; Burgess, A. R. Study of Some Medium Size Alcohols and Hydroperoxides by Photoelectron Spectroscopy. *J. Chem. Soc., Faraday Trans. 2* **1977**, *73*, 1247–1261.
- (23) Kimura, K.; Katsumata, S.; Achiba, Y.; Yamazaki, T.; Iwata, S. *Handbook of He(I) Photoelectron Spectra of Fundamental Organic Molecules*; Japan Scientific Societies Press, Tokyo, 1981.
- (24) Eland, J. H. D.; Berkowitz, J. Photoionization Mass Spectrometry of HI and DI at High Resolution. *J. Chem. Phys.* **1977**, *67*, 5034–5039.
- (25) Potts, A. W.; Williams, T. A. The Observation of “Forbidden” Transitions in He II Photoelectron Spectra. *J. Electron Spectrosc. Relat. Phenom* **1974**, *3*, 3–17.
- (26) Cradock, S.; Whiteford, R. A. Photoelectron Spectra of the Methyl, Silyl and Germyl Derivatives of the Group VI Elements. *J. Chem. Soc., Faraday Trans. 2* **1972**, *68*, 281–288.
- (27) Nakasgawa, H.; Asano, M.; Kubo, K. Mass Spectrometric Study of the Vaporization of Lithium Metasilicate. *J. Nucl. Mater.* **1981**, *102*, 292–297.

- (28) King, G. H.; Kroto, H. W.; Suffolk, R. J. The Photoelectron Spectrum of a Short-Lived Species in the Decomposition Products of CS₂. *Chem. Phys. Lett.* **1972**, *13*, 457–458.
- (29) Colbourne, D.; Frost, D. C.; McDowell, C. A.; Westwood, N. P. C. The Photoelectron Spectra of the Isoelectronic Molecules Hypochlorous Acid HOCl and Chloramine NH₂Cl. *J. Chem. Phys.* **1978**, *68*, 3574–3580.